PHILOSOPHICAL TRANSACTIONS A

rsta.royalsocietypublishing.org

Review

Cite this article: Alexandrov DV, Galenko PK, Toropova LV. 2018 Thermo-solutal and kinetic modes of stable dendritic growth with different symmetries of crystalline anisotropy in the presence of convection. *Phil. Trans. R. Soc. A* **376**: 20170215.
http://dx.doi.org/10.1098/rsta.2017.0215

Accepted: 18 September 2017

One contribution of 16 to a theme issue 'From atomistic interfaces to dendritic patterns'.

Subject Areas:
applied mathematics, mathematical modelling, complexity, mathematical physics, materials science

Keywords:
dendritic growth, phase transitions, kinetics, forced convection, selection theory, crystalline anisotropy

Author for correspondence:
Dmitri V. Alexandrov
e-mail: dmitri.alexandrov@urfu.ru

Thermo-solutal and kinetic modes of stable dendritic growth with different symmetries of crystalline anisotropy in the presence of convection

Dmitri V. Alexandrov[1], Peter K. Galenko[2] and Lyubov V. Toropova[1]

[1]Department of Theoretical and Mathematical Physics, Laboratory of Multi-Scale Mathematical Modelling, Ural Federal University, Ekaterinburg, 620000, Russian Federation
[2]Physikalisch-Astronomische Fakultät, Friedrich-Schiller-Universität Jena, 07743 Jena, Germany

DVA, 0000-0002-6628-745X; PKG, 0000-0003-2941-7742

Motivated by important applications in materials science and geophysics, we consider the steady-state growth of anisotropic needle-like dendrites in undercooled binary mixtures with a forced convective flow. We analyse the stable mode of dendritic evolution in the case of small anisotropies of growth kinetics and surface energy for arbitrary Péclet numbers and n-fold symmetry of dendritic crystals. On the basis of solvability and stability theories, we formulate a selection criterion giving a stable combination between dendrite tip diameter and tip velocity. A set of nonlinear equations consisting of the solvability criterion and undercooling balance is solved analytically for the tip velocity V and tip diameter ρ of dendrites with n-fold symmetry in the absence of convective flow. The case of convective heat and mass transfer mechanisms in a binary mixture occurring as a result of intensive flows in the liquid phase is detailed. A selection criterion that describes such solidification conditions is derived. The theory under consideration comprises previously considered theoretical approaches and results as limiting cases.

This article is part of the theme issue 'From atomistic interfaces to dendritic patterns'.

THE ROYAL SOCIETY PUBLISHING

1. Introduction

A tree-like crystal structure having a main stem with lateral branches that are formed along the crystallographic axes is called a dendrite (after the Greek word 'dendro' meaning 'tree') [1–4]. A dendritic shape represents the widely distributed crystal morphology appearing as a result of solidification processes in many undercooled melts and supersaturated solutions (see, among others, [5–9]). The growth kinetics and shapes of dendrites are controlled by heat and mass transfer processes and anisotropic properties of the crystal–liquid interface. Therefore, dendrites are formed in a broad range of microscopic, mesoscopic and macroscopic length scales, i.e. from 10^{-6} up to 10^{-3} m.

A number of experimental studies show that the internal structure of solidified materials (e.g. monocrystal or polycrystal) is highly dependent on the level of undercooling (supersaturation), solidification velocity and dendritic tip radius [4,10–14]. Therefore, the problem of the theoretical description of a stable dendritic growth mode, which is influenced by the crystal symmetry, kinetics, surface energy anisotropy and convection, represents one of the challenging tasks of materials physics [15–17]. This problem stems from the classical Ivantsov solutions [18,19] and experimental data [20–22] describing the steady-state growth of parabolic dendrites. A detailed theoretical analysis has demonstrated that the isotropic solutions found by Ivantsov are unstable, that is, the parabolic dendritic shape is unstable; however, the anisotropy of surface energy and atomic kinetics are capable of stabilizing the dendrite shape in close proximity to the parabolic Ivantsov solutions [23–25]. The Ivantsov solutions represent the main contribution, approximate a real dendritic shape and give the basis for selection analyses.

The pioneering result on the basis of solvability theory for the purely thermal problem of dendritic growth was obtained by Langer & Hong [26]. They found a combination (solvability criterion) $\sigma^* \equiv 2d_0 D_{\mathrm{T}}/(\rho^2 V) = \sigma_0 \alpha_d^{7/4}$ between the stable diameter ρ of the dendritic tip and its growth velocity V in the case of fourfold crystalline anisotropy, small Péclet number limit and $\alpha_d \ll 1$ (here d_0 is the capillary constant, D_{T} is the thermal diffusivity, α_d is the surface energy stiffness and σ_0 is a selection constant). Slightly later, this result was obtained by Pelcé & Bensimon [27], with the further generalization of this criterion for the fourfold symmetry of the crystal lattice by Ben Amar & Pelcé [28] for a binary system, by Bouissou & Pelcé [29] for a forced convective flow and for arbitrary Péclet numbers [30]. These solvability criteria have been joined together in the review paper on dendritic growth [31]. More recently, the effect of atomic kinetics for a high-rate solidification has been included [32]. In this work, the thermo-solutal and kinetically limited regimes of steady-state dendritic growth have been analysed. Some peculiarities of dendritic growth in diluted multicomponent systems were studied in [33] and in the Earth's inner core boundary in [34]. The theory of rapid dendritic solidification has been developed by stitching together different stability asymptotics [35,36], obtaining a criterion for σ^* valid for undercoolings up to several hundred kelvin [37]. The case of sixfold symmetry was studied just a little while ago [38] within the framework of thermally controlled dendritic solidification with a forced convective flow.

2. The model of dendritic growth

(a) Governing equations

Consider the steady-state growth of a two- and three-dimensional dendritic crystal along the spatial axis z in the presence of a forced convective flow coming from the opposite direction (figure 1). The phase transition temperature T_{int} at the dendrite interface is determined by the latent heat of solidification Q, specific heat c_p, the interface curvature $\mathcal{K}$, the anisotropic capillary length $d(\theta, \phi)$, the melting temperature T_{m} for the pure system and the intensity of atomic kinetics, given by the function of anisotropic kinetics $\tilde{\beta}(\theta, \phi)$ with the spherical angles θ and ϕ which define the orientation of the normal to the dendrite interface to its growth direction. The following

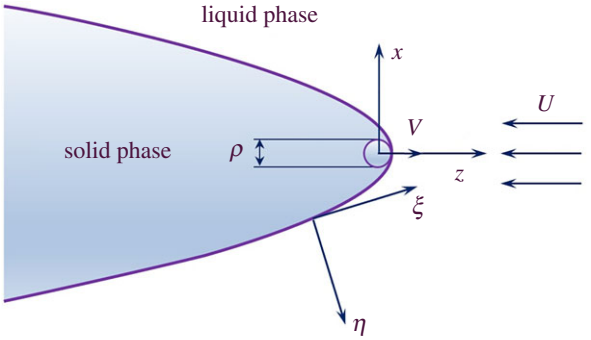

Figure 1. A sketch of dendritic growth in a forced convective flow. (Online version in colour.)

Gibbs–Thomson equation at the solid–liquid boundary holds:

$$T_{\rm int} = T_{\rm l} = T_{\rm s} = T_{\rm m} - mC_{\rm l} - T_Q d(\theta,\phi)\mathcal{K} - \tilde{\beta}(\theta,\phi)v_{\rm n}, \tag{2.1}$$

where $T_Q = Q/c_p$ is the hypercooling (temperature for adiabatic solidification), $v_{\rm n} = (\mathbf{v}\cdot\mathbf{n})$ is the normal growth velocity, $\mathbf{n}$ is the unit normal to the interface, m is the liquidus slope and $T_{\rm l}$ and $T_{\rm s}$ stand for the temperatures in liquid and solid. The curvature is given by

$$\mathcal{K} = \begin{cases} \dfrac{1}{R}, & \text{two-dimensional space,} \quad \text{2D case,} \\ \dfrac{(R_1+R_2)}{(R_1R_2)}, & \text{three-dimensional space,} \quad \text{3D case,} \end{cases} \tag{2.2}$$

where R is the dendrite tip radius in two dimensions and R_1 and R_2 are the main radii of curvature for a three-dimensional dendritic tip.

In the case of cubic symmetry, the capillary length $d(\theta,\phi)$ and the function of anisotropic kinetics $\tilde{\beta}(\theta,\phi)$ are described by

$$d(\theta,\phi) = d_0\{1-\alpha_d[\cos^4\theta + \sin^4\theta\,(1-2\sin^2\phi\cos^2\phi)]\} \tag{2.3}$$

and

$$\tilde{\beta}(\theta,\phi) = \beta_0\{1-\alpha_\beta[\cos^4\theta + \sin^4\theta\,(1-2\sin^2\phi\cos^2\phi)]\}, \tag{2.4}$$

where d_0 is the capillary constant, $\alpha_d \ll 1$ stands for the stiffness, which depends on a small anisotropy parameter ε_c of surface energy, β_0 is the kinetic constant and $\alpha_\beta \ll 1$ is the kinetic anisotropy parameter. Considering the case of a needle-like crystal in the form of a paraboloid of revolution, equation (2.3) can be reduced by averaging over ϕ as [39]: $d(\theta) = d_0\{1-\alpha_d\cos(4\theta)\}$ with the stiffness $\alpha_d = 15\varepsilon_c$ and the anisotropy ε_c of surface energy for cubic crystals. In this case, following the works [40,41], we assume that the selection criterion σ^* should have the scaling $\sigma^* \propto \alpha_d^{7/n}$ with the same exponent $7/n$ and the same general form if the anisotropy (2.3) or (2.4) are taken into account. Therefore, for obtaining the selection criterion σ^*, we shall use the simplest form of anisotropy under the assumption that the final scaling might be applied to three-dimensional dendritic growth in which $d(\theta)$ and $\tilde{\beta}(\theta)$ are written for the case of n-fold symmetry

$$d(\theta) = d_0\{1-\alpha_d\cos[n(\theta-\theta_d)]\}, \quad \tilde{\beta}(\theta) = \beta_0 T_Q\{1-\alpha_\beta\cos[n(\theta-\theta_\beta)]\}, \tag{2.5}$$

where θ_d and θ_β designate the angles between the directions of growth and minimal functions $d(\theta)$ and $\tilde{\beta}(\theta)$. Indeed, with $\theta = \theta_d$ and $\theta = \theta_\beta$ we have $\cos(\theta-\theta_d) = 1$, $\cos(\theta-\theta_\beta) = 1$ and $d(\theta)$ and $\tilde{\beta}(\theta)$ have minima due to the 'minus' signs in equation (2.5). As follows from equation (2.1), the maximum of $v_{\rm n}$ (largest undercooling and fastest growth) is reached by the growth direction consistent with the minimal values of $d(\theta)$ (that is, equivalent to the maximum of solid–liquid surface energy) and $\tilde{\beta}(\theta)$. An introduction of different angles in anisotropy has its

relevant meaning. Indeed, transitions between different growth directions have been obtained experimentally and explained by exchanging of anisotropies [12]. For the fourfold symmetric crystals, equations (2.5) were used in a numerical modelling by the boundary integral model [42] and in an analytical study by the non-local thermal conductivity problem [43] whose solution explains the transitions between growth directions due to the difference in angles θ_d and θ_β between anisotropies in different ranges of undercooling (supersaturation).

As a result of the above assumptions, instead of $d(\theta,\phi)$ and $\tilde{\beta}(\theta,\phi)$ we shall use $d(\theta)$ and $\tilde{\beta}(\theta)$ determined by equations (2.5) in the Gibbs–Thomson condition (2.1), in addition to which the following heat and mass balance conditions hold true at the dendritic interface:

$$T_Q(\mathbf{v}\cdot\mathbf{n}) = D_{\mathrm{T}}(\boldsymbol{\nabla}T_{\mathrm{s}} - \boldsymbol{\nabla}T_{\mathrm{l}})\cdot\mathbf{n} \tag{2.6}$$

and

$$(1-k_0)C_{\mathrm{l}}(\mathbf{v}\cdot\mathbf{n}) + D_{\mathrm{C}}\boldsymbol{\nabla}C_{\mathrm{l}}\cdot\mathbf{n} = 0, \tag{2.7}$$

where k_0 represents the equilibrium partition coefficient, C_{l} is the solute concentration in the liquid phase, and D_{C} represents the diffusion coefficient.

The convective heat and mass transport equations in the solid and liquid phases take the form

$$\frac{\partial T_{\mathrm{l}}}{\partial t} + (\mathbf{w}\cdot\boldsymbol{\nabla})T_{\mathrm{l}} = D_{\mathrm{T}}\nabla^2 T_{\mathrm{l}}, \quad \frac{\partial T_{\mathrm{s}}}{\partial t} = D_{\mathrm{T}}\nabla^2 T_{\mathrm{s}} \tag{2.8}$$

and

$$\frac{\partial C_{\mathrm{l}}}{\partial t} + (\mathbf{w}\cdot\boldsymbol{\nabla})C_{\mathrm{l}} = D_{\mathrm{C}}\nabla^2 C_{\mathrm{l}}, \tag{2.9}$$

where $\mathbf{w}$ is the fluid velocity. Here, we traditionally neglect atomic diffusion in the solid. For the sake of simplicity, we consider the case of equal thermal diffusivities in both phases. This hypothesis does not change the selection criteria given below due to the fact that different thermal diffusivities will change the selection constant only.

To describe the hydrodynamic flows, we use the linearized Oseen model for a viscous flow [44–46]

$$U\frac{\partial \mathbf{w}}{\partial z} = -\frac{1}{\rho_{\mathrm{l}}}\nabla p + \nu\nabla^2\mathbf{w}, \quad \nabla\cdot\mathbf{w} = 0. \tag{2.10}$$

Here, U is the fluid velocity far from the dendritic surface (see figure 1), p is the pressure, ρ_{l} is the density of the liquid and ν is the kinematic viscosity.

The convective heat and mass transfer problem (2.1)–(2.10) written out for the case of n-fold symmetry of crystal growth enables us to find the generalized solvability criterion, including the effects of kinetics and convection for arbitrary Péclet numbers. This criterion formulated below comprises previously known results and enables the theory for rapid solidification scenarios to be extended.

(b) Analytical solutions for a parabolic dendrite

In the present subsection, let us write out the Ivantsov solutions for the steady-state evolution of two- and three-dimensional parabolic dendrites in a forced convective flow. First of all, we define the corresponding parabolic coordinates ξ, η (and φ in three-dimensional geometry) connected with the Cartesian ones, x, y and z, by means of the familiar expressions

$$\left.\begin{aligned} &x = \rho\sqrt{\xi\eta}, \quad z = \frac{\rho}{2}(\eta-\xi), && \text{2D case,}\\ \text{and}\quad &x = \rho\sqrt{\xi\eta}\cos\varphi, \quad y = \rho\sqrt{\xi\eta}\sin\varphi, \quad z = \frac{\rho(\eta-\xi)}{2}, && \text{3D case,}\end{aligned}\right\} \tag{2.11}$$

where $\rho/2$ represents the dendritic tip radius, φ is the polar angle lying in the plane that is perpendicular to the incoming flow and equation $\eta = 1$ corresponds to the solid–liquid surface of the dendrite.

The Oseen hydrodynamic equations (2.10) supplemented by the corresponding no-slip boundary conditions for the fluid velocity components u_η, u_ξ (and u_φ in three-dimensional geometry) in the parabolic reference frame take the form [29,46]

$$\left.\begin{aligned} &u_\eta = -\frac{f_{2D}}{2\sqrt{\xi+\eta}}, \quad u_\xi = \frac{\sqrt{\xi\eta}}{\sqrt{\xi+\eta}}\frac{df_{2D}}{d\eta}, && \text{2D case,}\\ \text{and}\quad &u_\eta = -\frac{f_{3D}}{\sqrt{\xi+\eta}}, \quad u_\xi = \sqrt{\frac{\xi}{\xi+\eta}}\frac{d}{d\eta}\left(\sqrt{\eta}f_{3D}(\eta)\right), \quad u_\varphi = 0, && \text{3D case,} \end{aligned}\right\} \tag{2.12}$$

where

$$f_{2D}(\eta) = 2(U+V)\sqrt{\eta} - 2Ug_{2D}(\eta), \quad f_{3D}(\eta) = (U+V)\sqrt{\eta} - 2Ug_{3D}(\eta),$$

$$\text{and}\quad g(\eta) = \begin{cases} g_{2D}(\eta) = \sqrt{\eta}\dfrac{\operatorname{erfc}\sqrt{\eta Re/2}}{\operatorname{erfc}\sqrt{Re/2}} + \dfrac{\sqrt{2/(\pi Re)}}{\operatorname{erfc}\sqrt{Re/2}}\left[\exp\left(-\dfrac{Re}{2}\right) - \exp\left(-\dfrac{\eta Re}{2}\right)\right], & \text{2D,}\\ g_{3D}(\eta) = \dfrac{\sqrt{\eta}E_1(\eta Re/2)}{2E_1(Re/2)} + \dfrac{\exp(-Re/2) - \exp(-\eta Re/2)}{\sqrt{\eta}ReE_1(Re/2)}, & \text{3D,} \end{cases} \tag{2.13}$$

with the Reynolds number $Re = \rho U/\nu$.

Now rewriting the heat and mass transfer equations (2.8) and (2.9) as well as the boundary conditions (2.6) and (2.7) in parabolic coordinates, and then integrating them, we find the temperature and concentration distributions in two-dimensional and three-dimensional cases as

$$T_1(\eta) = T_i + (T_\infty - T_i)\frac{I_T(\eta)}{I_T(\infty)}, \quad C_1(\eta) = C_i + (C_{1\infty} - C_i)\frac{I_C(\eta)}{I_C(\infty)}, \tag{2.14}$$

where

$$\left.\begin{aligned} &I_T(\eta) = \int_1^\eta \exp\left[(j-1)P_f\int_1^{\eta'}\frac{g(\eta'')}{\sqrt{\eta''}}\,d\eta'' - P_0\eta'\right]\frac{d\eta'}{\eta'^{(j-1)/2}},\\ &I_C(\eta) = \int_1^\eta \exp\left[(j-1)P_f\frac{D_T}{D_C}\int_1^{\eta'}\frac{g(\eta'')}{\sqrt{\eta''}}\,d\eta'' - P_0\frac{D_T}{D_C}\eta'\right]\frac{d\eta'}{\eta'^{(j-1)/2}},\\ &T_i = T_\infty + T_Q P_g\exp(P_0)I_T(\infty), \quad P_0 = P_g + P_f,\\ \text{and}\quad &C_i = \frac{C_{1\infty}}{1-(1-k_0)\exp(P_0D_T/D_C)P_gI_C(\infty)D_T/D_C}, \quad E_1(q) = \int_q^\infty\frac{\exp(-u)}{u}\,du, \end{aligned}\right\} \tag{2.15}$$

T_∞ and $C_{1\infty}$ are the temperature and solute concentration in the liquid phase far from the dendrite surface, $P_g = \rho V/(2D_T)$ and $P_f = \rho U/(2D_T)$ stand for the growth and flow Péclet numbers, and $j = 2$ and $j = 3$ in the two- and three-dimensional geometry, respectively.

If a solidified dendrite is not infinitely symmetric about the axis of its growth as the paraboloid of revolution, the thermo-solutal Ivantsov solutions (2.14) and (2.15) should, in particular cases, be replaced by the Horvay–Cahn solutions [47,48], which are described in the accompanying paper in the present theme issue on the boundary integral theory [49].

3. Solvability integral and linear stability analysis

(a) Solvability condition

In the case of small anisotropies in surface energy and kinetics, the temperature and solute concentration distributions lie in close proximity to the parabolic Ivantsov solutions describing the steady-state dendritic growth. Pelcé & Bensimon [27] (see also [23,29]) showed that this statement leads to the microscopic solvability condition, which represents an approximate analytical solution of the linearized heat and mass transfer equations at the parabolic surface of Ivantsov's dendrite. As will be shown below, this solvability condition gives a unique

combination between ρ and V and describes a stable dendritic growth mode. After Pelcé & Bensimon [27] the solvability condition is given by

$$\int_{-\infty}^{\infty} G[X_0(l)]Y_m(l)\,\mathrm{d}l = 0, \quad Y_m(l) = \exp\left[\mathrm{i}\int_0^l k_m(l_1)\,\mathrm{d}l_1\right], \tag{3.1}$$

where G designates the curvature operator, $k_m(l)$ represents the marginal wavenumber mode, i is the imaginary unit and $X_0(l)$ is a continuum of solutions from which the dependence $k_m(l)$ can be derived. Expression (3.1) describes different shapes of evolving phase interfaces [23] and has the following meaning: the solution $G[X_0(l)]$ is orthogonal to the imposed perturbation $Y_m(l)$ that provides a stable mode. This condition follows from the Wentzel–Kramers–Brillouin method [50], which was also applied for flame propagation [51] and needle-like fronts of crystals [52].

(b) Stability analysis

For the sake of simplicity, let us initially develop the theory for the purely thermal problem. To obtain the marginal wavenumbers k_m entering the solvability integral (3.1), let us carry out a linear stability analysis. We assume that a perturbation caused by any kind of small fluctuations disturbs the liquid phase on a distance that is about the perturbation wavelength $2\pi/k_m$. Taking this into account, we expand the steady-state velocity components (2.12) in series in the small vicinity of dendrite $\eta = 1$. Keeping in mind the principal contributions only, we have

$$u_\eta = -\frac{V}{\sqrt{1+\xi}}, \quad u_\xi = \sqrt{\frac{\xi}{1+\xi}}[V + Ua(Re)(\eta - 1)], \tag{3.2}$$

where

$$a(Re) = \begin{cases} \sqrt{\dfrac{Re}{2\pi}}\dfrac{\exp(-Re/2)}{\operatorname{erfc}(\sqrt{Re/2})}, & \text{2D case,} \\ \dfrac{\exp(-Re/2)}{E_1(Re/2)}, & \text{3D case.} \end{cases} \tag{3.3}$$

For the sake of convenience, we introduce (after Bouissou & Pelcé [29]) the local Cartesian coordinates (x_c, y_c) fixed at the dendritic surface such that x_c and y_c, respectively, represent the tangent and normal directions to the dendrite interface at a point where the normal makes an angle θ with the growth direction. Using this frame of reference, one can express the velocity components and temperature gradient as

$$\bar{u} = -V\sin\theta - \frac{aU}{\rho}\sin\theta\cos\theta\, y_c, \quad \bar{v} = -V\cos\theta, \quad \frac{\mathrm{d}\bar{T}_\mathrm{l}}{\mathrm{d}y_c} = -\frac{T_Q V}{D_\mathrm{T}}\cos\theta. \tag{3.4}$$

Now let u', v', T'_l and T'_s designate the fluid velocity and temperature perturbations with respect to the stationary fields, whereas ξ' is the steady-state interface perturbation having a wavelength λ that is many times less than ρ. This enables us to neglect the advective term in the Oseen equations (2.10) and arrive at the following hydrodynamic equations for perturbations:

$$\boldsymbol{\nabla} p' = \nu\rho_\mathrm{l}\nabla^2\mathbf{w}', \quad \boldsymbol{\nabla}\cdot\mathbf{w}' = 0, \tag{3.5}$$

where p' and $\mathbf{w}'$ are the perturbations of pressure and fluid velocity.

The temperature perturbations in the liquid and solid phases follow from equations (2.8) and take the form

$$\frac{\partial T'_{\mathrm{l,s}}}{\partial t} + \bar{u}\frac{\partial T'_{\mathrm{l,s}}}{\partial x_c} + \bar{v}\frac{\partial T'_{\mathrm{l,s}}}{\partial y_c} + v'\frac{\mathrm{d}\bar{T}_{\mathrm{l,s}}}{\mathrm{d}y_c} = D_\mathrm{T}\nabla^2 T'_{\mathrm{l,s}}, \tag{3.6}$$

since the steady-state temperature distribution does not depend on x_c.

On the unperturbed solid–liquid boundary $y_c = 0$, one can obtain the following conditions for perturbations:

$$T'_{\mathrm{s}} = -T'_{\mathrm{l}} + \frac{T_Q V}{D_{\mathrm{T}}}\cos\theta\,\xi' = T_Q\, d(\theta)\frac{\partial^2\xi'}{\partial y_c^2} - \tilde{\beta}(\theta)\frac{\partial\xi'}{\partial t}, \quad u' = 0, \quad v' = -\frac{\partial\xi'}{\partial t},$$
$$\frac{T_Q}{D_{\mathrm{T}}}\frac{\partial\xi'}{\partial t} = \frac{\partial T'_{\mathrm{s}}}{\partial y_c} - \frac{\partial T'_{\mathrm{l}}}{\partial y_c} - \frac{T_Q V^2\cos^2\theta}{D_{\mathrm{T}}^2}\xi'. \tag{3.7}$$

Equations (3.5) imply that the pressure and velocity component perturbations can be expressed as

$$\left.\begin{aligned} p' &= 2\nu\rho_1 A\exp(\omega t + \mathrm{i}kx_c - \epsilon k y_c),\\ u' &= (B - \mathrm{i}\epsilon A y_c)\exp(\omega t + \mathrm{i}kx_c - \epsilon k y_c),\\ \text{and}\quad v' &= \left[A\left(y_c + \frac{\epsilon}{k}\right) + \mathrm{i}B\epsilon\right]\exp(\omega t + \mathrm{i}kx_c - \epsilon k y_c), \end{aligned}\right\} \tag{3.8}$$

where A and B stand for the amplitudes of perturbations, ω and k represent the frequency and wavenumber of perturbations, i is the imaginary unit and ϵ has the same sign as the real part of k because the perturbations cannot diverge at $y_c \to \infty$.

Substitution of perturbations (3.8) into the boundary conditions (3.7) defines A and B as

$$A = -C\left(\omega K\epsilon + \frac{\mathrm{i}akU\sin\theta\cos\theta}{\rho}\right), \quad B = \frac{CaU\sin\theta\cos\theta}{\rho}. \tag{3.9}$$

Here, C represents the amplitude of interface perturbation $\xi' = C\exp(\omega t + \mathrm{i}kx_c - \epsilon k y_c)$.

Further substitution of the temperature perturbations $T'_{\mathrm{s,l}} = \tilde{T}_{\mathrm{s,l}}\exp(\omega t + \mathrm{i}kx_c - \epsilon k y_c)$ (here $\tilde{T}_{\mathrm{s,l}}$ are the temperature amplitudes in the solid and liquid phases) into equations (3.6) and boundary conditions (3.7) leads to the dispersion law $\omega(k)$. This law at the neutral stability curve (where $\omega = 0$) leads to the marginal mode of wavenumber k_m (see, for details, [29,31]), which is determined by the following cubic equation:

$$k_m^3 = \frac{V\exp(\mathrm{i}\theta)}{2\,d(\theta)D_{\mathrm{T}}}k_m + \frac{\mathrm{i}aU\sin\theta\cos\theta}{8\rho D_{\mathrm{T}}}k_m - \frac{\mathrm{i}V\sin\theta}{2D_{\mathrm{T}}}k_m^2 + \frac{V^2\cos\theta\exp(\mathrm{i}\theta)}{4\,d(\theta)D_{\mathrm{T}}^2} + \frac{\mathrm{i}V\tilde{\beta}(\theta)\sin\theta}{d(\theta)T_Q}k_m^2. \tag{3.10}$$

The first summand on the right-hand side of expression (3.10) represents the well-known Mullins–Sekerka wavenumber [23,27]

$$k_{m\,\mathrm{MS}} = -\sqrt{\frac{V\exp(\mathrm{i}\theta)}{2\,d(\theta)D_{\mathrm{T}}}}, \tag{3.11}$$

while the first two contributions define the Bouissou & Pelcé expression [29,31]

$$k_{m\,\mathrm{BP}} = k_{m\,\mathrm{MS}}\sqrt{1 + \frac{\mathrm{i}aUd(\theta)}{8\rho V}\sin(2\theta)\exp(-\mathrm{i}\theta)}. \tag{3.12}$$

Furthermore, the first four contributions in (3.10) correspond to the high Péclet number scenario and determine the following wavenumber [30,32]:

$$k_{m\,\mathrm{AG}} = k_{m\,\mathrm{BP}} + \frac{V\exp(-\mathrm{i}\theta)}{4D_{\mathrm{T}}}. \tag{3.13}$$

The first and fifth terms on the right-hand side of expression (3.10) describe the kinetically limited crystal growth without convection studied by Brener [43].

An analytical solution of cubic equation (3.10) has been found using Cardano's formula ($d_0 \neq 0$) for the fourfold symmetry of dendritic growth as [32]

$$k_m = k_{m\,\mathrm{AG}} + \frac{\mathrm{i}V\tilde{\beta}(\theta)\sin\theta}{2\,d(\theta)T_Q}. \tag{3.14}$$

In the kinetically limited growth regime ($d_0 \to 0$), equation (3.10) leads to [32]

$$k_m = \frac{\mathrm{i}T_Q \exp(\mathrm{i}\theta)}{2D_\mathrm{T}\tilde{\beta}(\theta)\sin\theta} + \frac{V\cos\theta}{2D_\mathrm{T}}. \tag{3.15}$$

The aforesaid limiting cases (3.11)–(3.15) described by the single generalized expression (3.10) have been previously considered for the fourfold crystal growth symmetry ($n = 4$). Expression (3.10) transforms to the corresponding expression (3) for the sixfold symmetry ($n = 6$) [38].

(c) Solvability criterion for thermally controlled growth

Consider the purely thermal mode of dendritic solidification described by expression (3.14) when $\alpha_d \ll 1$, $\alpha_\beta \ll 1$, $\theta_d = 0$ and $\theta_\beta \neq 0$. Substituting the wavenumber (3.14) into the solvability integral (3.1), we arrive at

$$\int_{-\infty}^{\infty} \mathrm{d}\eta\, G[X_0(\eta)] \exp\left\{-\mathrm{i}\int_0^\eta \left[\frac{P_g(1-\mathrm{i}\eta_1)}{2} + \frac{\mathrm{i}\rho V\beta_0\eta_1}{2d_0} - \sqrt{\frac{(1+\mathrm{i}\eta_1)(1+\eta_1^2)^{\lambda_n} + \mathrm{i}\alpha\eta_1 B_n(\eta_1)}{\sigma^* B_n(\eta_1)}}\right]\mathrm{d}\eta_1\right\} = 0, \tag{3.16}$$

where

$$l_1 = -\frac{\rho}{2}\left[\frac{\tan\theta}{\cos\theta} + \ln\left(\frac{1}{\cos\theta} + \tan\theta\right)\right], \quad \eta = \tan\theta, \quad \alpha = \frac{aUd_0}{4\rho V}, \quad \lambda_n = \frac{n+1}{2}, \quad \sigma^* = \frac{2d_0D_\mathrm{T}}{\rho^2 V},$$

$$B_n(\eta) = (1+\eta^2)^{n/2} - \alpha_d \sum_{k=0}^{n} \binom{n}{k} \eta^{n-k} \cos\frac{(n-k)\pi}{2}.$$

Expression (3.16) contains previously constructed solvability theories [29,30,32] for the fourfold crystal growth symmetry (when $n = 4$). More specifically, expression (3.16) transforms to equations (39) and (40) obtained by Bouissou & Pelcé [29] at $n = 4$, $P_g \ll 1$ and $\beta_0 = 0$. In addition, the solvability integral (3.16) becomes identical to expression (5) from [30] and to equation (20) from [32] for the same conditions at arbitrary Péclet number.

The wavenumber in the kinetically limited regime can be obtained by combining relations (3.1) and (3.15) under the assumptions that $\theta_\beta = 0$ and $\theta_d \neq 0$:

$$\int_{-\infty}^{\infty} \mathrm{d}\eta\, G[X_0(\eta)] \exp\left\{-\mathrm{i}\int_0^\eta \left[P_g + \frac{\mathrm{i}\rho(1+\mathrm{i}\eta_1)(1+\eta_1^2)^{\lambda_n}}{2D_\mathrm{T}\beta_0\eta_1 B_n'(\eta_1)}\right]\mathrm{d}\eta_1\right\} = 0,$$

$$B_n'(\eta) = (1+\eta^2)^{n/2} - \alpha_\beta \sum_{k=0}^{n} \binom{n}{k} \eta^{n-k} \cos\frac{(n-k)\pi}{2}. \tag{3.17}$$

The integrals (3.16) and (3.17) become identical to integrals (20) and (24) from [32] for the fourfold dendritic symmetry ($n = 4$).

We calculate the solvability integral (3.16) in two stages as detailed in [32]. At the first stage, we neglect the kinetic contribution (proportional to β_0 in (3.16)) and pay attention to the case known as 'thermally controlled' crystal growth. Setting $\beta_0 = 0$, we come to the selection criterion

(see also [29–31])

$$\sigma^* = \frac{2d_0 D_T}{\rho^2 V} = \frac{\sigma_0 \alpha_d^{7/n} A_n^{7/n}}{(1 + a_1 \alpha_d^{2/n} A_n^{2/n} P_g)^2 (1 + b\tau_n^{\upsilon_n})}, \tag{3.18}$$

where

$$\tau_n = \alpha \alpha_d^{-3/n} A_n^{-3/n}, \quad \upsilon_n = \frac{n+7}{2(n+3)}, \quad A_n = 2^{-3n/4} \sum_{k=0}^{n} \binom{n}{k} \mathrm{i}^{n-k} \cos \frac{(n-k)\pi}{2},$$

and σ_0 and b are constants. Indeed, if we consider the fourfold crystal symmetry, when $A_4 = 1$ and $\upsilon_4 = \frac{11}{14}$, the generalized criterion (3.18) transforms to the previously known results (see criterion (6) in [30] and criterion (25) in [32]). If this is really the case, a_1 is given by [30]

$$a_1 = \left(\frac{8\sigma_0}{7}\right)^{1/2} \left(\frac{3}{56}\right)^{3/8}.$$

The second stage to evaluate the integral expression (3.16) is to analyse the dendrite growth mode controlled by the kinetic contribution (proportional to β_0). By doing so, we neglect the summand proportional to the growth Péclet number in (3.16) and arrive at (by analogy with [32])

$$\sigma^* = \frac{\sigma_0 \alpha_d^{7/n} A_n^{7/n}}{[1 + a_1' \alpha_d^{2/n} P_g D_T \beta_0 A_n^{2/n}/d_0]^2 (1 + b\tau_n^{\upsilon_n})}, \tag{3.19}$$

where a_1' is a new constant previously found for the fourfold symmetry ($n = 4$) [32,43]

$$a_1' = 20\sqrt{\frac{\sigma_0}{3}}.$$

The obtained criterion (3.19) becomes identical to the asymptotic criterion (25) given by Brener [43] for $n = 4$, $U = 0$ and if the second contribution in square brackets in its denominator is many times greater than unity. The derived criterion (3.19) is identical to criterion (26) deduced in [32] merely at $n = 4$.

Stitching together the obtained limiting criteria (3.18) and (3.19), we come to the generalized criterion of the form

$$\sigma^* = \frac{\sigma_0 \alpha_d^{7/n} A_n^{7/n}}{[1 + a_1 \alpha_d^{2/n} A_n^{2/n} P_g (1 + \delta_0 D_T \beta_0/d_0)]^2 (1 + b\tau_n^{\upsilon_n})}, \tag{3.20}$$

where $a_1' = a_1 \delta_0$ and δ_0 represents a fitting constant. Note that the selection constants σ_0 and b for each n might be found experimentally or from the phase-field modelling by analogy with the fourfold growth symmetry ($n = 4$) studied in [53–56].

Keeping in mind that $\sigma^* = 2d_0 D_T/(\rho^2 V) = d_0 V/(2D_T P_g^2)$, let us reformulate the selection criterion (3.20) in terms of the dendrite tip velocity V as

$$V = \frac{2D_T P_g^2 \sigma_0 \alpha_d^{7/n} A_n^{7/n}/d_0}{[1 + a_1 \alpha_d^{2/n} A_n^{2/n} P_g (1 + \delta_0 D_T \beta_0/d_0)]^2 (1 + b\tau_n^{\upsilon_n})}. \tag{3.21}$$

Expression (3.21) coincides with the expression $V \propto D_T \alpha_d^{3/4} d_0^{-1} f(\sqrt{\alpha_d} P_g)$ previously obtained in [57] for a motionless liquid phase with $n = 4$ (the reader may find the function f in figure 8 in [57]).

The derived criteria (3.20) and (3.21) entirely correspond to the previously obtained criteria (29) and (30) in [32] for $n = 4$. The difference between them is the powers of α_d and τ_n responsible for anisotropy and convection.

The generalized selection criteria (3.20) and (3.21) comprise previously studied growth regimes in a single-component melt with $n = 4$ and $n = 6$. In particular, equations (3.20) and (3.21) include the following criteria:

(i) without convection and growth kinetics for small Péclet number ($\alpha = 0$, $\beta_0 = 0$, $P_g \ll 1$, $n = 4$) [26,27];

(ii) without growth kinetics for small Péclet number ($\beta_0 = 0$, $P_g \ll 1$, $n = 4$) [29,31];
(iii) without convection and growth kinetics for arbitrary Péclet number ($\alpha = 0$, $\beta_0 = 0$, $n = 4$) [30,58];
(iv) without convection for small Péclet number ($\alpha = 0$, $P_g \ll 1$, $n = 4$) [43];
(v) with convection, anisotropy for $n = 4$ and $n = 6$ [32,38].

Finally, consider a regime with a predominant role of kinetic anisotropy. For the limiting case of small kinetic anisotropy $\alpha_\beta \ll 1$ in condition (3.17), we arrive at the selection criterion

$$V = \frac{\sigma_0 \alpha_\beta^{5/n} A_n^{5/n} P_g}{\beta_0 (1 + h_n \alpha_\beta^{2/n} A_n^{2/n} P_g)}. \tag{3.22}$$

This criterion describes the kinetically limited dendritic solidification occurring at large Péclet numbers only, where h_n is a constant. Consequently, assuming $P_g \gg 1$ in criteria (3.21) and (3.22), and equating them, we find h_n as

$$h_n = \frac{d_0 \alpha_\beta^{3/n} a_1^2 (1 + \delta_0 D_T \beta_0 / d_0)^2}{2 D_T \beta_0 \alpha_d^{3/n}}.$$

In the case of fourfold symmetry, $n = 4$, this formula transforms to the previously known one [32]. The criterion (3.22) can be reformulated for the dendrite tip diameter ρ as

$$\rho = \frac{2 D_T \beta_0 (1 + h_n \alpha_\beta^{2/n} A_n^{2/n} P_g)}{\sigma_0 \alpha_\beta^{5/n} A_n^{5/n}}. \tag{3.23}$$

Criteria (3.22) and (3.23) are identical to expressions (35) and (36) from [32] for $n = 4$. In addition, expression (3.22) transforms to criterion (16) from [43] if the growth Péclet number is small enough. Indeed, with the given kinetic anisotropy, α_β, the tip radius (3.23) depends on the growth Péclet number in the whole range of the growth velocity. By contrast, using estimations $h_n < 1$ and $\alpha_\beta^{2/n} < 1$, the limiting regime of small growth Péclet numbers, $P_g \ll 1$, can be deduced from equation (3.22) as $V = \sigma_0 \alpha_\beta^{5/n} A_n^{5/n} P_g / \beta_0$. This result has been obtained by equation (16) in Brener [43] for fourfold symmetry, $n = 4$, which is equivalent to the expression

$$\rho = \frac{2 D_T \beta_0}{\sigma_0} \alpha_\beta^{-5/n} A_n^{-5/n},$$

showing that, for a given kinetic anisotropy, α_β, the dendrite tip radius takes a constant value for each arbitrarily chosen dendrite tip velocity. Thus, both criteria (3.22) and (3.23) confirm a key role of kinetics (when compared with the surface energy anisotropy) for high-rate dendritic growth highlighted in [59,60].

(d) Solvability criteria for solutal and thermo-solutal growth

Consider now a chemical dendrite in a binary mixture growing in the presence of convection under constant temperature. The problem statement and solvability analysis are quite similar to the aforementioned purely thermal theory. The difference consists in the fact that the chemical dendrite is described by the so-called one-sided model (diffusion in the liquid controls the growth and diffusion in the solid is negligible). This gives a scale factor '2' in the solvability criterion. In addition, keeping in mind a correlation multiplier $mC_i(1 - k_0)/T_Q$ appearing as a result of transition from the purely thermal to the purely chemical Stefan problem, we come to the stability criterion σ^*_{CD} that describes a stable dendritic growth in two-component isothermal systems with

a forced convective flow:

$$\sigma^*_{\mathrm{CD}} = \frac{2d_0D_{\mathrm{C}}}{\rho^2V} = \frac{[2mC_i(1-k_0)/T_{\mathrm{Q}}]\sigma_0\alpha_d^{7/n}A_n^{7/n}}{[1+a_2\alpha_d^{2/n}A_n^{2/n}P_{\mathrm{C}}(1+\delta_0D_{\mathrm{C}}\beta_0/d_{0\mathrm{CD}})]^2(1+b\tau_{n\mathrm{CD}}^{\upsilon_n})}, \tag{3.24}$$

where

$$\tau_{n\mathrm{CD}} = \frac{\alpha_{\mathrm{CD}}}{\alpha_d^{3/n}A_n^{3/n}}, \quad \alpha_{\mathrm{CD}} = \frac{aUd_{0\mathrm{CD}}}{2\rho V}, \quad d_{0\mathrm{CD}} = \frac{T_{\mathrm{Q}}d_0}{2mC_i(1-k_0)}, \quad P_{\mathrm{C}} = \frac{\rho V}{2D_{\mathrm{C}}}$$

and $a_2 = \sqrt{2}a_1$ [30].

The two selection criteria (3.20) and (3.24) derived for thermally and chemically stable dendritic growth should be joined together into a unified criterion for the thermo-solutal problem. A complete deduction of this criterion for the fourfold symmetry is given in [31]. The unified selection criterion, which gives a combination between V and ρ for dendritic growth in binary systems with a forced convection and takes into account the anisotropies of growth kinetics and surface energy, reads as

$$\sigma^* = \frac{2d_0D_{\mathrm{T}}}{\rho^2V} = \frac{\sigma_0\alpha_d^{7/n}A_n^{7/n}}{1+b\bar{\tau}_n^{\upsilon_n}}\left\{\frac{1}{[1+a_1\alpha_d^{2/n}A_n^{2/n}P_g(1+\delta_0D_{\mathrm{T}}\beta_0/d_0)]^2}\right.$$
$$\left. + \frac{2mC_i(1-k_0)D_{\mathrm{T}}}{[1+a_2\alpha_d^{2/n}A_n^{2/n}P_{\mathrm{C}}(1+\delta_0D_{\mathrm{C}}\beta_0/d_{0\mathrm{CD}})]^2T_{\mathrm{Q}}D_{\mathrm{C}}}\right\}, \tag{3.25}$$

where

$$\bar{\tau}_n = \alpha_d^{-3/n}A_n^{-3/n}\left(\frac{aUd_0}{4\rho VP} + \frac{aUd_0D_{\mathrm{T}}}{2\rho VPD_{\mathrm{C}}}\right), \quad P = 1 + \frac{2mC_i(1-k_0)D_{\mathrm{T}}}{T_{\mathrm{Q}}D_{\mathrm{C}}}.$$

The criterion (3.25) works at arbitrary Péclet numbers within the framework of the parabolic heat and mass transfer model. What is most remarkable is that this criterion contains previously studied limiting cases. In addition to limits described in its thermal part (3.20) (the first summand in curly brackets of expression (3.25)), the criterion (3.25) includes the following modes:

(vi) without convection and growth kinetics for small Péclet number and constant temperature ($\alpha = 0$, $\beta_0 = 0$, $P_g \ll 1$) [28];
(vii) for the thermo-solutal problem with fourfold symmetry [30–32].

4. Undercooling balance

In this section, the second relation for V and ρ via the undercooling balance is formulated. This second relation and selection criterion allow us to obtain a pair of most important parameters of primary solidification, V and ρ, at a unique undercooling ΔT.

(a) Governing equations

The thermo-solutal criterion (3.25) obtained for the n-fold symmetry determines the first combination between the crystal tip velocity V and its tip diameter ρ as $\sigma^* = 2d_0D_{\mathrm{T}}/(\rho^2V)$. This combination is the result of solutions lying close to the steady-state Ivantsov or Horvay–Cahn solutions, which determine the temperature and concentration at the surface of the two- or three-dimensional dendrite.

The second combination between V and ρ is found from the undercooling balance, which represents the driving force of crystal growth. The total undercooling $\Delta T = T_{\mathrm{m}} - T_\infty$ at the dendrite tip consists of several contributions:

$$\Delta T = \Delta T_{\mathrm{T}} + \Delta T_{\mathrm{C}} + \Delta T_{\mathrm{R}} + \Delta T_{\mathrm{K}}, \tag{4.1}$$

where ΔT_{T} and ΔT_{C} stand for the thermal and solutal undercoolings, $\Delta T_{\mathrm{R}} = 2d_0T_{\mathrm{Q}}/R$ is the undercooling appearing due to the Gibbs–Thomson effect and $\Delta T_{\mathrm{K}} = V/\mu_k$ represents the kinetic

undercooling (μ_k is the kinetic coefficient). The total undercooling balance (4.1) connects the surface temperature T_i at the dendritic tip and the far-field temperature T_∞.

Introducing the modified thermal and solutal Ivantsov functions

$$\left.\begin{aligned} &\mathrm{Iv}^*_\mathrm{T}(P_g,P_f)=P_g\exp(P_0)I_\mathrm{T}(\infty),\quad P_0=P_g+P_f,\\ \text{and}\quad &\mathrm{Iv}^*_\mathrm{C}(P_\mathrm{C},P_{cf})=P_\mathrm{C}\exp(P_\mathrm{C}+P_{cf})I_\mathrm{C}(\infty),\end{aligned}\right\} \tag{4.2}$$

the thermal and solutal contributions are given by

$$\left.\begin{aligned} &\Delta T_\mathrm{T}=T_Q\mathrm{Iv}^*_\mathrm{T}(P_g,P_f),\\ \text{and}\quad &\Delta T_\mathrm{C}=\frac{mC_\infty(1-k_0)\mathrm{Iv}^*_\mathrm{C}(P_\mathrm{C},P_{cf})}{1-(1-k_0)\mathrm{Iv}^*_\mathrm{C}(P_\mathrm{C},P_{cf})},\end{aligned}\right\} \tag{4.3}$$

where $P_{cf}=\rho U/(2D_\mathrm{C})$. Expressions (4.1)–(4.3) represent an implicit combination for V and ρ as functions of ΔT.

(b) Exact analytical solutions

The set of two equations (3.25) and (4.1) determine the stable mode of crystal growth in a two-component mixture. In the absence of convection, $U=0$, this set of two equations can be resolved analytically. Indeed, the thermal and concentration integrals (2.15) depend on the growth Péclet number P_g only,

$$I_\mathrm{T}(P_g)=\int_1^\infty\frac{\exp(-P_g\eta')}{\eta'^{(j-1)/2}}\,\mathrm{d}\eta',\quad I_\mathrm{C}(P_g)=\int_1^\infty\frac{\exp(-P_gD_\mathrm{T}\eta'/D_\mathrm{C})}{\eta'^{(j-1)/2}}\,\mathrm{d}\eta', \tag{4.4}$$

as well as the modified Ivantsov functions (4.2),

$$\mathrm{Iv}^*_\mathrm{T}(P_g)=P_g\exp(P_g)I_\mathrm{T}(P_g),\quad \mathrm{Iv}^*_\mathrm{C}(P_g)=\frac{P_gD_\mathrm{T}}{D_\mathrm{C}}\exp\left(\frac{P_gD_\mathrm{T}}{D_\mathrm{C}}\right)I_\mathrm{C}(P_g). \tag{4.5}$$

Then, the surface concentration C_i, undercooling ΔT_i and $d_{0\mathrm{CD}}$ also depend on P_g:

$$\left.\begin{aligned} &C_i(P_g)=\frac{C_{l\infty}}{1-(1-k_0)\mathrm{Iv}^*_\mathrm{C}(P_g)},\quad \Delta T_i(P_g)=\frac{(1-k_0)mC_i(P_g)}{k_0T_Q}\\ \text{and}\quad &d_{0\mathrm{CD}}(P_g)=\frac{T_Qd_0}{2mC_i(P_g)(1-k_0)}.\end{aligned}\right\} \tag{4.6}$$

Therefore, the solvability criterion (3.25) reads

$$\begin{aligned}\frac{d_0}{\sigma_0\alpha_d^{7/n}A_n^{7/n}\rho P_g}&=\frac{1}{[1+a_1\alpha_d^{2/n}A_n^{2/n}P_g(1+\delta_0D_\mathrm{T}\beta_0/d_0)]^2}\\&+\frac{2k_0\Delta T_i(P_g)D_\mathrm{T}}{[1+a_2\alpha_d^{2/n}A_n^{2/n}P_g(1+\delta_0D_\mathrm{C}\beta_0/d_{0\mathrm{CD}}(P_g))D_\mathrm{T}/D_\mathrm{C}]^2D_\mathrm{C}}\equiv\Lambda(P_g).\end{aligned} \tag{4.7}$$

Equation (4.7) can be rewritten to obtain the dendrite tip diameter as a function of P_g:

$$\rho(P_g)=\frac{d_0}{\sigma_0\alpha_d^{7/n}A_n^{7/n}P_g\Lambda(P_g)}. \tag{4.8}$$

Keeping in mind the parametric solutions (4.4)–(4.8) and expressing velocity V in terms of P_g,

$$V(P_g)=\frac{2D_\mathrm{T}P_g}{\rho(P_g)}, \tag{4.9}$$

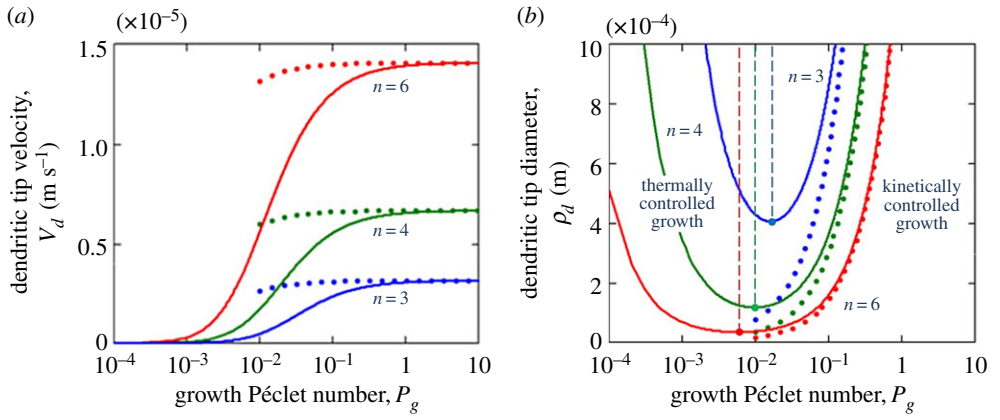

Figure 2. Dimensionless dendritic tip velocity $V_d = Vd_0/D_T$ and diameter $\rho_d = \rho/d_0$ as functions of the growth Péclet number P_g. Physical parameters are [32]: $\sigma_0 = 2$, $U = 0$, $\alpha_d = \alpha_\beta = 0.1$, $D_T\beta_0/d_0 = 20$, $a_1 = 0.5$, $\delta_0 = 32.4$. The solid and dashed curves are plotted for $\theta_d = 0$ and $\theta_\beta = 0$, respectively. The crystal growth symmetry is marked as $n = 6$ (red), $n = 4$ (green) and $n = 3$ (blue). The vertical lines plotted through the minimum points for each curve divide the parametric regions of thermally controlled and kinetically limited regimes. (Online version in colour.)

we reformulate the undercooling balance (4.1) in a parametric form of P_g as

$$\Delta T = \Delta T_T(P_g) + \Delta T_C(P_g) + \frac{4d_0T_Q}{\rho(P_g)} + \frac{2D_TP_g}{\mu_k\rho(P_g)}, \tag{4.10}$$

where

$$\Delta T_T(P_g) = T_Q \mathrm{Iv}^*_T(P_g), \quad \Delta T_C(P_g) = \frac{mC_\infty(1-k_0)\mathrm{Iv}^*_C(P_g)}{1-(1-k_0)\mathrm{Iv}^*_C(P_g)}.$$

Concluding this section, expressions (4.8)–(4.10) represent the exact parametric solutions (with the parameter P_g) in the absence of convective flow.

(c) Behaviour of solutions

Figure 2 illustrates dimensionless dendrite tip velocity $V_d = Vd_0/D_T$ and tip diameter $\rho_d = \rho/d_0$ calculated by analytical solutions (4.8) and (4.9). The solid curves demonstrate the thermally controlled growth, which is described by selection criteria (3.20), (3.21) or (3.25), while the dotted lines show the kinetically limited growth, which is defined by selection criteria (3.22) and (3.23).

First, the dendritic crystals having larger growth symmetry (large values of n) evolve faster than the corresponding crystals having smaller n (see figure 2*a*). As this takes place, their tip diameter ρ is smaller, that is, the crystals are thinner than those with smaller n. Second, the minima of curves plotted in figure 2*b* highlight a transition from thermally controlled growth to kinetically limited growth. The thermally controlled growth (the solid curves in figure 2) asymptotically tends to the kinetically limited growth (the dotted curves in figure 2) with increasing growth Péclet number. Third, the velocity and tip diameter given by the selection criteria (3.20) and (3.21) for the thermally controlled growth smoothly tend to their values given by selection criteria (3.22) and (3.23) for the kinetic regime. Meanwhile, expressions (3.20), (3.21) and (3.25) have been derived for the growth mode governed by the surface energy anisotropy α_d, while expressions (3.22) and (3.23) have been obtained for the mode controlled by the kinetic anisotropy α_β. In other words, these two groups of selection criteria define two physically different solidification scenarios. Note that in the nearly asymptotic region ($10^{-1} \lesssim P_g \lesssim 1$) the growth velocity can sharply change between the thermally controlled and kinetically limited regimes (i.e. between the solid and dotted lines in figure 2). This takes up the question of what is the selection growth mode between kinetic and thermal branches illustrated in figure 2. Will

this transition be smooth or discontinuous[1] in the behaviour of V and ρ? Answers to these questions might be found in natural experiments with the solidification of transparent liquids and in computational modelling of rapid dendritic growth.

5. Dendritic growth under convective heat and mass transport at the interface

The fluid velocity field in the vicinity of growing dendrites might be so intensive that it may lead to convective heat and mass transport fluxes at the dendritic surface [61]. The conductive mechanism of heat and mass transfer (2.6) and (2.7) becomes inapplicable. For developing the selection of growth mode under intensive convective conditions, we consider below the corresponding theory for the fourfold symmetry ($n = 4$) in the presence of so-called convective heat and mass fluxes in the liquid phase [61–67]. Such fluxes can be caused, for instance, by turbulent mixing in the oceanic boundary layer underneath the ice cover.

Let us especially note that in the case of dendritic growth in electromagnetically levitated undercooled droplets, it is possible to observe solidification processes with high Reynolds numbers of the order of 10^2–10^3 [68,69]. This experimental evidence is confirmed by the following estimation of the Reynolds number. If we choose typical dendritic parameters such as dendrite tip diameter approximately 10^{-5}–10^{-6} m, fluid velocity approximately 10^{-5}–1 m s^{-1} and kinematic viscosity approximately 10^{-7} m^2 s^{-1}, we come to the Reynolds number approximately 10^{-4}–10^3, which corresponds to experimental data [68,69]. In other words, if we are dealing with undercooled metallic melts, one can expect that the heat and mass transfer mechanism becomes convective and, as is shown in [68], the fluid flow inside the levitated drop becomes turbulent. These estimations of course are valid only outside a narrow boundary layer surrounding the growing dendritic structures. As a result, an important task for future investigations is to estimate the Reynolds number in this boundary layer. We will not dwell on this point below, where the theory of a stable mode of dendritic growth is developed with allowance for convective boundary conditions at the phase interface.

(a) The model and its steady-state solution

If the flow near the dendrite surface is substantial, the rate of its motion depends on the convective (or turbulent) fluxes of heat and solute in the liquid phase (ocean). In this case, the boundary conditions (2.6) and (2.7) of heat and mass balance at the dendrite interface are replaced by [61,62,64,65]

$$\frac{T_Q}{D_\mathrm{T}}\mathbf{v}\cdot\mathbf{n} = \nabla T_\mathrm{s}\cdot\mathbf{n} + \frac{\alpha_h \rho_\mathrm{l} c_\mathrm{l} u_*}{k_\mathrm{s}}(T_i - T_\infty) \tag{5.1}$$

and

$$(1-k_0)C_i\mathbf{v}\cdot\mathbf{n} = \alpha_m u_*(C_i - C_{\mathrm{l}\infty}), \tag{5.2}$$

where subscript i designates the temperature and solute concentration at the dendrite interface, α_h and α_m are the convective (turbulent) coefficients for heat and mass, ρ_l and c_l are the density and specific heat capacity of the liquid phase, k_s is the thermal conductivity coefficient of the solid phase and u_* represents the friction velocity (see figure 3). Note that the friction velocity is determined as $u_* = \sqrt{\tau_\mathrm{s}/\rho_\mathrm{l}}$, where τ_s is the shear stress [71]. The ratio of exchange coefficients α_h/α_m depends on the molecular diffusivities for heat D_T and impurity D_C, so that $\alpha_h/\alpha_m = (D_\mathrm{T}/D_\mathrm{C})^{\bar{n}}$ [61,66] with $\frac{2}{3} < \bar{n} < \frac{4}{5}$ [72–74].

Equations (2.8) and (2.9) must be integrated in parabolic coordinates (2.11) with allowance for the boundary conditions (5.1) and (5.2). The integration leads to the temperature and concentration distributions (2.14), where I_T, I_C, T_i and C_i are determined by the following

[1]According to the work of Brener [43], the transition between thermally controlled and kinetically limited regimes can be smooth or sharp depending on the preferred growth directions along the anisotropy of surface energy, α_d, or along the anisotropy of kinetics, α_β.

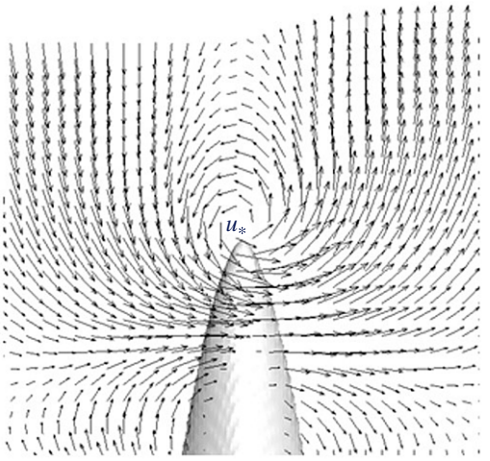

Figure 3. Schematic representation of a curl induced by intensive convective flow far from a dendritic interface. The curl provides convective transport of heat and mass (expressions (5.1) and (5.2)) and friction velocity u_* at the dendritic surface. The distribution of velocities, shown in this curl by arrows, is taken from Gao *et al.* [70]. (Online version in colour.)

expressions:

$$\left.\begin{aligned} I_{\mathrm{T}}(\eta) &= \int_1^{\eta} \frac{\exp(-P_g\eta')}{\eta'^{(j-1)/2}}\,\mathrm{d}\eta', \quad I_{\mathrm{C}}(\eta) = \int_1^{\eta} \frac{\exp(-P_{\mathrm{C}}\eta')}{\eta'^{(j-1)/2}}\,\mathrm{d}\eta', \\ \text{and} \qquad T_i &= T_\infty + \frac{T_Q V k_{\mathrm{s}}}{\alpha_h \rho_{\mathrm{l}} c_{\mathrm{l}} u_* D_{\mathrm{T}}}, \quad C_i = \frac{\alpha_m u_* C_{\mathrm{l}\infty}}{\alpha_m u_* - (1-k_0)V}, \end{aligned}\right\} \tag{5.3}$$

with $j=2$ and $j=3$ in the two- and three-dimensional cases (as before).

(b) Linear stability analysis for convective boundary conditions

As has already been mentioned, analytical solutions describing the steady-state dendritic growth can be found in the vicinity of steady-state solutions (2.14) and (5.3) in the case of small anisotropies of surface energy and growth kinetics. In order to find the marginal mode for wavenumber k_m, one can develop the linear stability analysis in the case of convective heat and mass transfer mechanisms by analogy with the previous description. The temperature perturbations T_{l}' and T_{s}' are governed by equation (3.6), whereas the concentration perturbation C_{l}' has a similar form when replacing D_{T} by D_{C} and T_{l}' by C_{l}'. As $U=0$ in the present model (hydrodynamic flows are characterized by the friction velocity u_* only, figure 3), $\bar{u}$ and $\bar{v}$ from (3.4) have only the main contributions, i.e. $\bar{u}=-V\sin\theta$ and $\bar{v}=-V\cos\theta$.

In accordance with the aforementioned theory, temperature and concentration perturbations ($T_{\mathrm{l,s}}'$ and C_{l}') as well as the dendritic interface perturbation (ξ') take the form

$$\left.\begin{aligned} & T_{\mathrm{l}}' = (T_{\mathrm{l}0} + T_{\mathrm{l}1}y_c + T_{\mathrm{l}2}y_c^2)E(t,x_c,y_c), \quad T_{\mathrm{s}}' = (T_{\mathrm{s}0} + T_{\mathrm{s}1}y_c + T_{\mathrm{s}2}y_c^2)E(t,x_c,y_c), \\ \text{and} \qquad & C' = (C_0 + C_1y_c + C_2y_c^2)E(t,x_c,y_c), \quad \xi' = CE(t,x_c,y_c), \end{aligned}\right\} \tag{5.4}$$

where, as before, ϵ has the same sign as the real part of k, $\partial\xi'/\partial t = -v'$ at the surface, and $E(t,x_c,y_c)=\exp(\omega t + \mathrm{i}kx_c - \epsilon k y_c)$; $T_{\mathrm{l}\iota}$, $T_{\mathrm{s}\iota}$, C_ι and C represent the amplitudes of perturbations ($\iota=0,1,2$).

Substitution of solutions (5.4) into the temperature and concentration perturbation equations leads to

$$\left.\begin{aligned} T_{1,s2} &= \frac{\omega C}{4D_T}\frac{d\bar{T}_{1,s}}{dy_c}, \quad T_{1,s1} = \frac{3\omega C}{4\epsilon k D_T}\frac{d\bar{T}_{1,s}}{dy_c} - \frac{[\omega + Vk(\epsilon\cos\theta - i\sin\theta)]T_{1,s0}}{2\epsilon k D_T}, \\ \text{and} \qquad C_2 &= \frac{\omega C}{4D_C}\frac{d\bar{C}_1}{dy_c}, \quad C_1 = \frac{3\omega C}{4\epsilon k D_C}\frac{d\bar{C}_1}{dy_c} - \frac{[\omega + Vk(\epsilon\cos\theta - i\sin\theta)]C_0}{2\epsilon k D_C}. \end{aligned}\right\} \tag{5.5}$$

Solutions (5.5) transform to the corresponding expressions in the limiting case of zero velocity of a laminar flow previously found in [31]. The derivatives $d\bar{T}_1/dy_c = h_1$ and $d\bar{C}_1/dy_c = h_2$ at the dendrite surface $y_c = 0$ entering in (5.5) can be obtained from the steady-state solutions (2.14) and (5.3) as

$$h_1 = -\frac{2T_Q V k_s \exp(-P_g)}{\rho\alpha_h\rho_1 c_1 u_* D_T I_T(\infty)}, \quad h_2 = -\frac{2(1-k_0)VC_{1\infty}\exp(-P_C)}{\rho[\alpha_m u_* - (1-k_0)V]I_C(\infty)}. \tag{5.6}$$

Now, expanding the boundary conditions (2.1), (5.1) and (5.2) in series, we come to the following set of conditions imposed at the dendritic interface $y_c = 0$:

$$\left.\begin{aligned} T_1' &= -(h_1 + mh_2)\xi' - mC_1' - d_T Q\frac{\partial^2\xi'}{\partial y_c^2} + \tilde{\beta}\frac{\partial\xi'}{\partial t}, \\ T_s' &= mh_2\xi' + mC_1' + d_T Q\frac{\partial^2\xi'}{\partial y_c^2} - \tilde{\beta}\frac{\partial\xi'}{\partial t}, \quad \frac{T_Q}{D_T}\frac{\partial\xi'}{\partial t} = \frac{\partial T_s'}{\partial y_c} - 2bh_1\xi' - 2bT_1', \\ \text{and} \qquad & \frac{1-k_0}{\alpha_m u_*}\left(V\cos\theta\, C_1' + V\cos\theta\, h_2\xi' + C_i\frac{\partial\xi'}{\partial t}\right) + C_1' + h_2\xi' = 0, \end{aligned}\right\} \tag{5.7}$$

where $b = \alpha_h\rho_1 c_1 u_*/(2k_s)$.

Further substitution of perturbations (5.4) into the boundary conditions (5.7) leads to four equations for the perturbation amplitudes T_{1l0}, T_{s0}, C_0 and C. Equating the determinant of this system to zero, we get a dispersion equation for the function $\omega(k)$. Now consider a coordinate system moving in a normal direction to the dendrite interface with velocity $V\cos\theta$. Owing to the rotational symmetry of the system a perturbation with wavenumber k grows with rate $\omega(k)$. However, if the origin of the coordinate system is moving along the z-axis with the constant velocity V, the perturbation grows as $\omega(k) - iVk\sin\theta$ by the action of the tangential velocity $V\sin\theta$ in the new reference frame [29]. Therefore, replacing $\omega(k)$ by $-iVk\sin\theta$ at the neutral stability curve (where ω vanishes), setting $\epsilon = -1$ and substituting $-i$ instead of i according to the previous theories [29–32], we come to the following equation for the wavenumber marginal mode $k = k_m$:

$$k^2 + \left(2b - \frac{i\beta V\sin\theta}{d} - \frac{iB\sin\theta}{dA}\right)k - \frac{2bi\beta V\sin\theta}{d} - \frac{iV\sin\theta}{D_T d} - \frac{2biB\sin\theta}{dA} = 0, \tag{5.8}$$

where

$$A = 1 + \frac{(1-k_0)V\cos\theta}{\alpha_m u_*}, \quad B = \frac{(1-k_0)mC_i V}{\alpha_m u_* T_Q}, \quad \beta(\theta) = \frac{\tilde{\beta}(\theta)}{T_Q}.$$

(c) Solvability criterion

(i) Purely thermal growth

For the dendritic growth in a one-component system without impurities ($C_{1\infty} = C_i = 0$), one can find the following expression for the wavenumber from equation (5.8):

$$k = -b\sqrt{1 + \frac{iqV\sin\theta}{bd}} - b + \frac{i\beta V\sin\theta}{2d}, \tag{5.9}$$

where we assume that $\alpha_\beta \ll 1$, $V \lesssim 10\,\mathrm{m\,s^{-1}}$ and $q = \beta_0 + 1/(bD_T)$. Now substituting k from (5.9) into the solvability condition (3.1) in the case of small anisotropy parameters ($\alpha_d \ll 1$ and $\alpha_\beta \ll 1$)

and with a zero angle between the directions of growth and surface energy minimum (with $\theta_d = 0$, see explanations around equation (2.5)), one can obtain

$$\int_{-\infty}^{\infty} \mathrm{d}\phi\, G[X_0(\eta(\phi))] \exp\left\{ \int_{1/\sqrt{2\alpha_d}}^{\phi} \left[\sqrt{\frac{2^{7/4}\rho^2 bqV\alpha_d^{5/4}(\phi'^{5/2} - \tilde{\tau}\phi(\phi'^2 - 1))}{d_0(1-\phi'^2)}} + \frac{\rho}{\sqrt{2\alpha_d} d_0}\left(2^{7/4}\alpha_d^{5/4} b d_0 \sqrt{\phi'} + \beta_0 V \alpha_d^{3/4}\right)\right] \mathrm{d}\phi' \right\}, \tag{5.10}$$

where the following notations are introduced [23,27,29,31]:

$$l_1 = -\frac{\rho}{2}\left[\frac{\tan\theta}{\cos\theta} + \ln\left(\frac{1}{\cos\theta} + \tan\theta\right)\right], \quad \tan\theta = \mathrm{i}(1 - \sqrt{2\alpha_d}\phi') = \eta(\phi'), \quad \tilde{\tau} = \frac{2^{3/4}\alpha_d^{1/4} b d_0}{qV}.$$

The solvability integral (5.10) can be found in accordance with the previous theory developed in [23,27,29,31]. Two dominant contributions exist for this integral: the contribution from the loop and the contribution from the stationary phase points. The first contribution should be calculated between a distance $\sim \tilde{\tau}^{2/3}$ (a splitting distance of the stationary phase points) at the intersection of the steepest descent path and the real axis and $\phi' \sim 1$. This contribution leads to an oscillating factor to the exponentially small value of the integral of the form

$$\cos\left[\bar{A}_1 \sqrt{\frac{\alpha_d^{5/4} D_\mathrm{T} bq}{\sigma^*}}(1 + \bar{B}_1 \tilde{\tau}^{3/2}) + \frac{2b_1\tilde{\tau}}{3} + b_2\tilde{\tau}^{2/3}\right],$$

$$\sigma^* = \frac{2d_0 D_\mathrm{T}}{\rho^2 V}, \quad b_1 = 2^{5/4}\alpha_d^{3/4}\rho b, \quad b_2 = \frac{\alpha_d^{1/4}\rho\beta_0 V}{\sqrt{2}d_0}. \tag{5.11}$$

The contribution from the stationary phase points has the following oscillating part:

$$\cos\left[\bar{A}_2 \sqrt{\frac{\alpha_d^{5/4} D_\mathrm{T} bq}{\sigma^*}}(1 + \bar{B}_2 \tilde{\tau}^{3/2}) + \frac{2b_1(1-\tilde{\tau})}{3} + b_2(1 - \tilde{\tau}^{2/3})\right]. \tag{5.12}$$

Here, $\bar{A}_1, \bar{A}_2, \bar{B}_1$ and $\bar{B}_2$ are constants. The cancellation of the sum of contributions (5.11) and (5.12) leads to the selection criterion for solely thermal dendritic growth in the presence of convective heat transfer in the liquid phase:

$$\sigma^* = \frac{\sigma_0 \alpha_d^{5/4}(1 + bD_\mathrm{T}\beta_0)(1 + \mu\tilde{\tau}^{3/2})^2}{[1 + \nu_1(\alpha_d^{3/4}\rho b + 3\alpha_d^{1/4}\rho\beta_0 V/2^{5/4}d_0)]^2}, \tag{5.13}$$

where σ_0, μ and ν_1 represent new constants.

The constant ν_1 can be determined from the limiting case of high growth velocities when the crystal grows in the kinetic regime. Indeed, setting $b \to 0$, $\tilde{\tau} \to 0$ and $3\nu_1\alpha_d^{1/4}\rho\beta_0 V/(2^{5/4}d_0) \gg 1$, equation (5.13) gives

$$\sigma^* = \frac{2^{1/2}\sigma_0\alpha_d^{3/4} d_0^2}{9\nu_1^2\beta_0^2 D_\mathrm{T}^2 P_g^2}, \quad P_g = \frac{\rho V}{2D_\mathrm{T}}. \tag{5.14}$$

The selection criterion previously found for the dendritic growth in a laminar forced flow (expression (29) in [32]) in the same limit takes the form

$$\sigma^* = \frac{\sigma_0\alpha_d^{3/4} d_0^2}{\gamma\beta_0^2 D_\mathrm{T}^2 P_g^2}, \quad \gamma = \frac{400\sigma_0}{3}. \tag{5.15}$$

Combining expressions (5.14) and (5.15), we get

$$\nu_1^2 = \frac{2^{9/2}25\sigma_0}{27}.$$

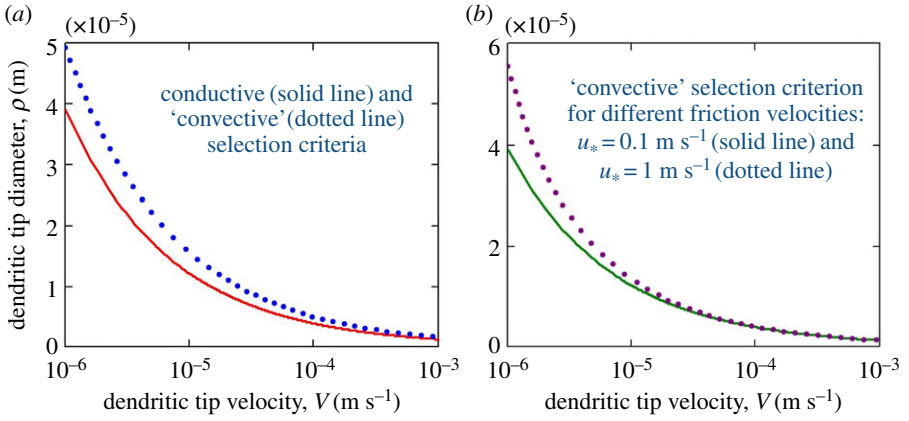

Figure 4. Panel (*a*) shows a comparison of selection criteria for the conductive heat transfer mechanism (3.20) (plotted for $n = 4$ and $U = 0$) and for the convective heat transfer mechanism (5.13) induced by intensive fluid motions (plotted for $u_* = 0.1\,\mathrm{m\,s^{-1}}$). Panel (*b*) compares the 'convective' selection criterion (5.13) at different friction velocities. Physical parameters are [38,62,74]: $\alpha_h = 0.0095$, $k_s = 2.03\,\mathrm{W\,m^{-1}\,{}^\circ C^{-1}}$, $\rho_l = 10^3\,\mathrm{kg\,m^{-3}}$, $c_l = 4187\,\mathrm{W\,s\,kg^{-1}\,{}^\circ C^{-1}}$, $d_0 = 2.8 \times 10^{-10}\,\mathrm{m}$, $\alpha_d = 0.35$, $\sigma_0 = 0.17$, $D_T = 1.17 \times 10^{-7}\,\mathrm{m^2\,s^{-1}}$, $\mu = 0$ and $\beta_1 = \beta_0 = 0$. (Online version in colour.)

Thus, the selection criterion (5.13) contains only two constants, σ_0 and μ, which should be determined from experimental data or phase field modelling [54,55].

The obtained 'convective' selection criterion (5.13) and the criterion (3.20) for the traditional conductive heat transfer mechanism in the liquid phase have a very similar behaviour $V(\rho)$ as is shown in figure 4*a*. It can be seen that the dendrite tip diameter is greater in the case of the convective heat transfer mechanism induced by intensive convective (even turbulent) motions in liquid (ocean) at a given crystal growth rate V. In addition, in the case of 'convective' growth conditions, the dendrite tip diameter increases with increasing friction velocity u_* at a fixed value of V (see figure 4*b*).

(ii) Thermo-solutal growth

To obtain a stability criterion for binary systems, we consider two different cases. The first case concerns very diluted systems, when $\beta_1 = \beta_0 + mC_i(1-k_0)/(T_Q\alpha_s u_*) \ll \sqrt{d_0/(VD_T)}$ or $\beta_1 \ll bd_0/V$ and $A \sim 1$ (the last estimation follows from the boundary condition (5.2)). In this limit, the wavenumber for the marginal mode takes the form of expression (5.9), where β_0 is replaced by $\beta_0 + mC_i(1-k_0)/(T_Q\alpha_s u_*)$. In this case, derivation of the stability criterion is completely analogous to the aforementioned case of pure systems and σ^* takes the form of expression (5.13), where we write β_1 instead of β_0:

$$\sigma^* = \frac{\sigma_0\alpha_d^{5/4}(1+bD_T\beta_1)(1+\mu\tilde{\tau}_1^{3/2})^2}{[1+\nu_1(\alpha_d^{3/4}\rho b + 3\alpha_d^{1/4}P_g\beta_1 D_T/2^{1/4}d_0)]^2}, \quad \tilde{\tau}_1 = \frac{\alpha_d^{1/4}\rho b^2 d_0}{2^{1/4}P_g(1+bD_T\beta_1)}. \tag{5.16}$$

The limit of applicability of this criterion is $\beta_1 \ll \sqrt{d_0/(VD_T)}$ or $\beta_1 \ll bd_0/V$.

The wavenumber for the marginal mode in the opposite limiting case $\beta_1 \gg \sqrt{d_0/(VD_T)}$ can be found from equation (5.8) in the form of

$$k = \frac{\mathrm{i}\beta_1 V \sin\theta}{d}. \tag{5.17}$$

Substituting k from (5.17) into the solvability condition (3.1) we obtain

$$\int_{-\infty}^{\infty} \mathrm{d}\phi\, G[X_0(\eta(\phi))] \exp\left(\frac{\sqrt{2\alpha_d}\rho V\beta_1}{d_0}\int_{1/\sqrt{2\alpha_d}}^{\phi}\frac{\phi'^2\,\mathrm{d}\phi'}{\phi'^2-1}\right). \tag{5.18}$$

The integral (5.18) is dominated by the contribution from the loop [29], which gives an oscillating factor to the exponentially small value of the integral,

$$\cos\left(\frac{\bar{A}_3\sqrt{\alpha_d}\rho V\beta_1}{d_0}\right),$$

where $\bar{A}_3$ is a constant. This function vanishes for selected values of the argument. Then, equating the last expression to zero, we obtain the criterion

$$\sigma^* = \frac{2d_0D_T}{\rho^2V} = \frac{\sigma_0\sqrt{\alpha_d}V\beta_1}{P_g} = \frac{2\sigma_0\sqrt{\alpha_d}D_T\beta_1}{\rho}, \tag{5.19}$$

where, again, σ_0 designates a constant, which must be found from experiments or phase field modelling. Note that the limit of applicability of criterion (5.19) is $\beta_1 \gg \sqrt{d_0/(VD_T)}$.

Let us especially emphasize that σ^* from expression (5.16), which is formally valid for $\beta_1 \ll \sqrt{d_0/(VD_T)}$, tends to zero for large β_1. On the other hand, σ^* from (5.19), which was derived in the limit $\beta_1 \gg \sqrt{d_0/(VD_T)}$, formally tends to zero for small β_1. This behaviour enables us to get a single solvability criterion by stitching together both limiting cases in β_1, i.e. expressions (5.16) and (5.19). Thus, the generalized criterion becomes

$$\sigma^*(\rho,V) = \frac{2d_0D_T}{\rho^2V} = \frac{\sigma_0\alpha_d^{5/4}(1+bD_T\beta_1)(1+\mu\tilde{\tau}_1^{3/2})^2}{[1+\nu_1(\alpha_d^{3/4}\rho b + 3\alpha_d^{1/4}P_g\beta_1D_T/2^{1/4}d_0)]^2} + \frac{2\sigma_0\sqrt{\alpha_d}D_T\beta_1}{\rho}. \tag{5.20}$$

Thus, selection criterion (5.20) determines a combination between V and ρ in the case of anisotropic thermo-solutal dendritic growth with allowance for the convective heat and mass transport mechanism in the liquid.

(d) Undercooling balance and exact analytical solution

The undercooling balance $\Delta T = T_m - T_\infty$ is defined by expression (5.20). Its contributions, as can be easily seen from (5.3), take the form

$$\Delta T_T = T_i - T_\infty = \frac{T_QVk_s}{\alpha_h\rho_1c_1u_*D_T}, \quad \Delta T_C = m(C_i - C_{l\infty}) = \frac{(1-k_0)VmC_{l\infty}}{\alpha_mu_* - (1-k_0)V}, \tag{5.21}$$

with, as before, $\Delta T_R = 4d_0T_Q/\rho$, and $\Delta T_K = V/\mu_k$ ($R = \rho/2$). Expressions (5.21) demonstrate that ΔT_T and ΔT_C are independent of ρ. Keeping in mind that the total undercooling $\Delta T = T_m - T_\infty$ is constant and combining equations (4.1) and (5.21), one can express the explicit function $\rho(V)$ in the form

$$\rho(V) = \frac{4d_0T_Q}{\Delta T - \Delta T_T(V) - \Delta T_C(V) - V/\mu_k}. \tag{5.22}$$

Now substituting $\rho(V)$ from (5.22) into (5.20), we come to the implicit equation for the dendritic velocity V of the form

$$\frac{\rho^2(V)V}{2d_0D_T}\sigma^*(\rho(V),V) = 1, \tag{5.23}$$

where $\sigma^*(\rho(V),V)$ is determined by the right-hand side of equation (5.20) after substituting $\rho(V)$ from expression (5.22). Thus, relations (5.22) and (5.23) represent the exact analytical solution if the convective heat and mass transport completely define the stable dendritic growth. Namely, equation (5.23) gives $V(\Delta T)$ and then equation (5.22) explicitly leads to the function $\rho(\Delta T)$.

6. The role of convection in dendrite growth kinetics

Convection plays an essential role in the growth of dendrites [15,16,75]. Convection may influence (i) the transport of heat and substances [46,53,76,77] as well as (ii) mechanical deformation of dendritic crystals [78]. Because the mechanical influence of the flow is not considered in this work, only the effect of the convective transport on the dendrite growth kinetics [79] is presented.

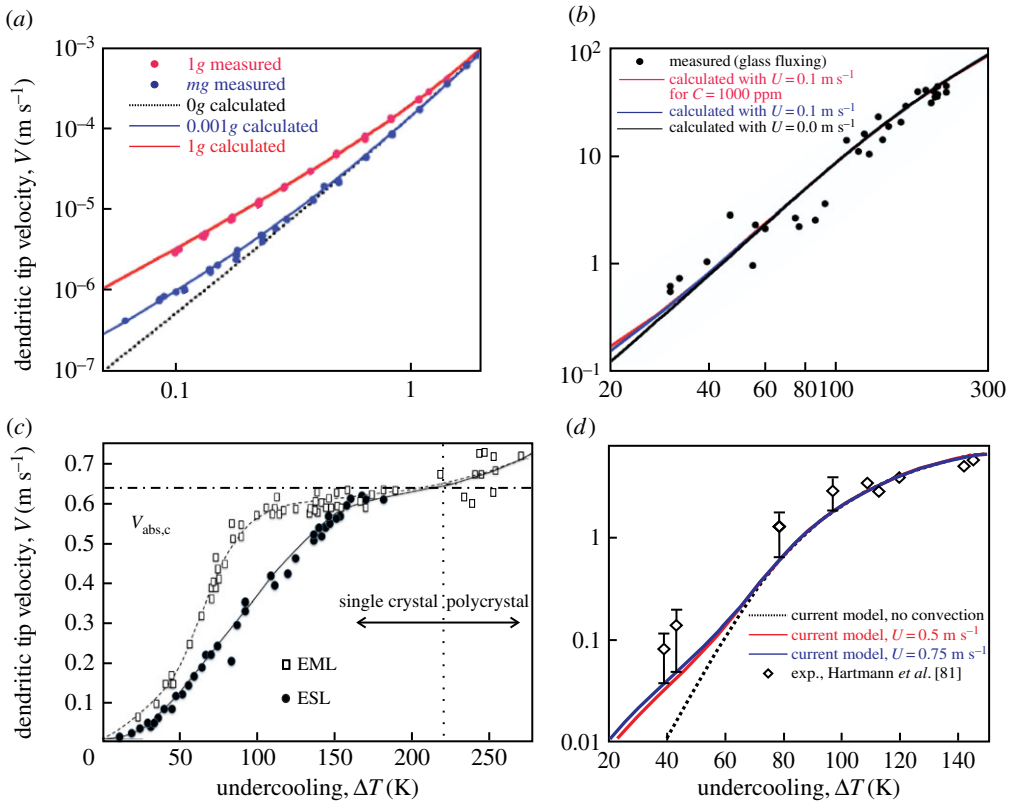

Figure 5. (*a*) Comparison of measured [80] and calculated [56] velocities of the growing SCN dendrites. (*b*) Calculated dendritic tip velocities (curves are given by Alexandrov & Galenko model [31]) in the glass-fluxed sample of pure nickel. For comparison, calculated tip velocities in the presence of a flow of 0.1 m s^{-1} and/or a strongly partitioning impurity of 1000 ppm are also shown. The measured tip velocities taken from Gao *et al.* [56] are plotted as functions of the measured and corrected undercoolings in Gao *et al.* [70]. (*c*) Dendrite growth velocities as functions of undercooling of Ni_2B alloy for various fluid flow velocities [13]. Electrostatic levitation (ESL, solid circles), $U = 0.00$ m s^{-1}, and EML (open squares), $U = 0.25$ m s^{-1}. With the increase of undercooling, the transition from irregular skeletal crystal to dendrite polycrystal ensemble occurs at the velocity of absolute chemical stability $V = V_{abs}$. (*d*) Calculation of growth velocities by the model [36] (lines) using various levels of convection ($U = 0, 0.5, 0.75$ m s^{-1}) in comparison with dendrite growth measurements (diamonds) of Hartmann *et al.* [81] for solidification of the $Ti_{45}Al_{55}$ alloy. Experimental error bars are shown only for the four smallest values of undercooling. (Online version in colour.)

To demonstrate the effect of convective transport on the growth kinetics, we have chosen four different materials: succinonitrile (SCN, a non-metallic and transparent substance) [80], nickel (a typical metal having face-centred-cubic crystalline lattice) [70], Ni_2B (a congruently melting alloy that solidifies without chemical segregation) [76] and $Ti_{45}Al_{55}$ (an alloy solidifying with chemical segregation) [81]. Figure 5 shows that in these four cases convection increases the dendrite growth velocity. Experimental data with convection exhibit higher dendrite growth velocity in comparison with data obtained for growth with (almost) negligible convection. Qualitatively, the more intensive growth occurs due to the joint action of conductive and convective heat and mass transports [82,83]. One quantitative explanation of the effect is that the thermal and/or solutal boundary layer shrinks due to convection, which results in a higher thermal and/or solutal gradient at the tips of dendrites and, therefore, in an increase of their velocity [15,77].

The theory [30] (see equation (3.25) with $n = 4$) has been tested against data for both velocity V and tip radius $\rho/2$ measured during growth of SCN dendrites under microgravity and terrestrial

conditions. As has been shown [56], V and $\rho/2$ are both sensitive to the action of flow, which can be well described theoretically in comparison with experimental data of Koss *et al.* [80]. Figure 5*a* demonstrates that the growth velocity of SCN dendrites is described by a theory that takes into account a negligible level of convection ($U = 0$, growth under microgravity) and an essential level of convection with velocity comparable to the dendrite velocity (growth on the ground).

The thermal history, flow pattern and dendritic structure of a glass-fluxed nickel sample have recently been modelled by magnetohydrodynamics calculations [70]. Simulations of temperature distribution and flow structure revealed a large thermal gradient crossing the sample, which led to an underestimation of the real undercooling for dendritic growth in the bulk volume of the sample. By accounting for this underestimation, the dendritic tip velocities in the glass-fluxed nickel melt have been calculated using a theory of three-dimensional dendritic growth with convection [31] (see equations (3.18) and (4.1)–(4.3) with $n = 4$) with an agreement between experiment and theory. Figure 5*b* shows the good fit the theory with incoming flow ($U > 0$) between and experimentally measured velocities of dendrites grown in the glass-fluxed nickel sample.

Convection affects not only the velocity but also the growth shape and even the crystal morphology [84]. As is shown in Binder *et al.* [13], undercooled drops of the Ni_2B alloy solidified in an electrostatic levitator (ESL) have a regular structure with macroscopically rounded dendrite tips, suggesting atomically rough growing facets. By contrast, Ni_2B alloy samples solidified in an electromagnetic levitator (EML) have a monocrystalline facetted structure suggesting atomically smooth growing facets. Such an Ni_2B monocrystal has a skeletal morphology [76] analogous to the known morphology of bismuth crystals. The structure of an Ni_2B skeletal crystal is irregular and grows in a convective flow at the undercooling $\Delta T < 225\,\mathrm{K}$, i.e. in the ΔT region to the left of the dotted vertical line in figure 5*c*. At higher undercoolings, $\Delta T > 225\,\mathrm{K}$, when the influence of convection decays due to the high crystal growth velocity, skeletal morphology and facetted shape are succeeded by a dendritic polycrystal ensemble (in the ΔT region to the right of the dotted vertical line in figure 5*c*). As a result, forced convection increases the growth velocity of Ni_2B crystals, stabilizes the growth of atomically smooth facets and changes the macroscopic growth shape [13]. More specifically, the crystal habit alters, i.e. a skeletal monocrystal acquires a dendritic structure as its growth velocity increases. Using the model of Alexandrov & Galenko [31] (see equations (3.18) and (4.1)–(4.3) with $n = 4$), theoretical predictions quantitatively agree with experimental crystal growth velocities with convection (EML data) and without convection (ESL data), see figure 5*c*.

The non-isothermal forced flow together with solute segregation may drastically influence the dendrite growth [36]. This is illustrated in the semi-log plot shown in figure 5*d*, where a systematic deviation of experimental data from theoretical predictions at the smallest values of undercooling and zero convective flow $U = 0$ can be seen. This deviation occurs in the range of growth velocity, $V \lesssim 1\,\mathrm{m\,s^{-1}}$, comparable with the estimated flow velocity in $Ti_{45}Al_{55}$ droplets processed in EML [13,69]. In this range, convection may drastically affect the growth kinetics due to comparable values of growth velocity V and flow velocity U [85,86]. Including an incoming flow $U > 0$ into the selection criterion of the stable growth mode increases the dendrite growth velocity, which leads to a decrease in this discrepancy if $V \approx U$. It is clearly apparent that at a flow velocity of $U = 0.75\,\mathrm{m\,s^{-1}}$ the model [36] is able to quantitatively reproduce the experimental results within the experimental margin of error given in Hartmann *et al.* [81]. Finally, one should note that the intensity of convection and flow velocity U were not measured directly in the experiments of Hartmann *et al.* [81] and so were not included in the list of measurable parameters. In this sense, the theoretical model of the work [36] uses the fluid velocity U as a parameter that relates to the process of viscous flow in levitated droplets realistically, but this parameter corresponds to the adjustment of theoretical predictions with respect to the experimental data independently of experimentally measured parameters.

Figure 5 demonstrates the effect of convection of the growth of dendrites with the *fourfold symmetry* of their crystal lattice ($n = 4$). In addition to this, equations (3.20) and (4.1)–(4.3) can also be tested regarding the influence of convective flow and *sixfold anisotropy* ($n = 6$). Growing in

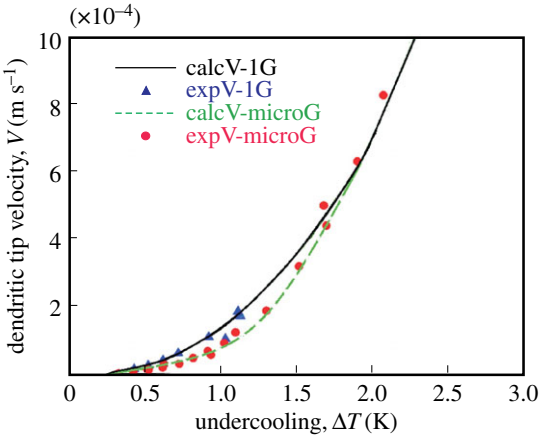

Figure 6. The velocity $V(\Delta T)$ of ice dendrite growing from undercooled water D_2O. The solid curve is given by the model with convective flow [38] and compared with data obtained on the ground (triangles [7]). The dashed curve is given by the model without convection [38] whose predictions are compared with data obtained on the International Space Station (circles [7]). (Online version in colour.)

undercooled water, secondary arms of ice dendrites evolve with the angle of 60° to the main stems of these dendrites, which indicates the preferable growth of crystals having sixfold symmetry. Using experimental data of Furukawa and co-workers [7] for dendrites grown from undercooled water D_2O under terrestrial and microgravity conditions, the model with and without convective heat transport given in the work [38] can be checked. Figure 6 shows a comparison for the tip velocity of an ice dendrite growing on the ground ($1g$ conditions) and in microgravity on board the International Space Station. It is clearly shown that convection increases the growth velocity, which is in good agreement with theoretical predictions. As in the case of dendrite growth with fourfold symmetry (see figure 5), this means that convection increases the thermal flux from the interface at which the latent heat releases during crystal growth. This result is consistent with the previous experimental results and theoretical advancements on the growth of pure and alloying dendrites [13,15,36,70,76,82].

Concluding this section, we should point out that figures 5 and 6 clearly show the increase of growth kinetics in the range of action of convective transport. This feature predicted by the theoretical models for growth of dendrites under convective flow in pure liquids and alloy melts is in agreement with experimental findings under terrestrial and reduced gravity conditions in EML and ESL facilities and with the use of the melt fluxing technique [70,76].

7. Final remarks

(a) Assumptions and simplifications of the theory

(i) Heat and mass transport

The statement of the problem given by equations (2.1)–(2.10) implies that the chemical segregation coefficient k_0, impurity diffusion coefficient D_C, liquidus slope m, liquid phase density ρ_l and kinematic viscosity ν are constants that do not depend on temperature and chemical composition. Moreover, thermal diffusivities in the phases are assumed to be similar, which allows one to directly employ the available methods for the description of dendrite growth [24,27,39]. Such a simplified statement of the problem ensues from the fact that, in particular, the difference

between thermal diffusivities enters the 'empirical constant' σ_0 of the condition being sought for the selection of the stable dendrite growth regime.

Extending the theory to the very wide range of solidification velocity (as stated in §§2 and 4), these simplifications can be crucial for the analysis and interpretation of experimental data. For instance, at high solidification rates, the liquidus line slope and chemical segregation coefficient become velocity-dependent functions, leading to a drastic change of growth kinetics, and making the transition from the diffusion-limited to thermally controlled growth very sharp [87]. However, these simplifications enable us to carry out the analytical calculations for systems of nonlinear equations with hydrodynamic contributions.

(ii) Flow

The Oseen approximation used in the equation of motion (2.10) makes it possible to take into account only the most important inertial terms. Even though calculations yield sufficiently accurate results in the literature on classical problems for a viscous fluid [31,45], the Oseen approximation may give an essential error in a quantitative description of two-dimensional flows [44,45]. However, the Oseen approximation is the only approximation which leads to the analytical solution for a needle-like dendrite in the presence of viscous flow. Following the approach developed by Bouissou & Pelcé [29], we extend their theory to three dimensions and show that it is possible to reach a good description of experimental data on crystal growth in a pure metallic melt (nickel), congruently melting alloy (Ni_2B) and organic transparent liquid (SCN) [13,56,76] (see figure 5). In addition, equations for the velocity field $\mathbf{w}$ and the mass conservation described by the Oseen approximation (2.10) assume the pressure p in the form

$$p = p_0 + \rho_0 g z[1 - \beta_T(T_{tip} - T_\infty)], \tag{7.1}$$

where ρ_0 is the fluid density at $T_{tip} = T_\infty$, i.e. if the temperature T_{tip} of the dendrite tip is equal to the temperature T_∞ far from the tip in the liquid phase, $\eta = \nu\rho_0$ is the dynamic viscosity, ν is the kinematic viscosity, g is the projection of gravitational acceleration on the coordinate axis z and β_T is the thermal expansion coefficient. In the quasi-stationary regime of dendrite growth with constant velocity, we assume that the difference $T_{tip} - T_\infty$ is constant. Therefore, the form of equations (2.10) and (7.1) allows us to describe various regimes of solidification with convection including (i) pure forced convection, $p_0 \gg |\rho_0 g z \beta_T(T_{tip} - T_\infty)|$, and (ii) natural convection, $p_0 \ll |\rho_0 g z \beta_T(T_{tip} - T_\infty)|$. In order to solve the problem of dendritic growth with natural convection, one should replace the conductive heat and mass transport conditions at the dendrite surface by the corresponding convective transfer boundary conditions [61] (see §5).

(iii) Anisotropy

The anisotropic capillary length $d(\theta, \phi)$ and the function of anisotropic kinetics $\tilde{\beta}(\theta, \phi)$ have been chosen by expressions (2.3) and (2.4) for fourfold cubic symmetry. Then, equations (2.3) and (2.4) have been reduced to their simplest form of anisotropy, $d(\theta)$ and $\tilde{\beta}(\theta)$, under the assumption that they are independent of the angle ϕ (due to infinite rotational symmetry of the paraboloidal dendrite) and the final scaling law for σ might be applied to three-dimensional dendritic growth in the case of n-fold symmetry (for the functions $d(\theta, \phi)$ and $\tilde{\beta}(\theta, \phi)$ given by equation (2.5)). For many symmetries, however, such an assumption has no geometrical and physical relevance. This assumption has just been used to obtain the selection criterion σ^* by the easiest and fastest route even though we have included in the analysis, for instance, sixfold symmetric crystals, which cannot also be described by the simplest approximation of the cubic crystalline lattices[2]. Therefore, special tests of the criterion (3.25) with regard to its applicability to dendrite crystals with different n-symmetries would be appropriate to check this approximation.

[2]Indeed, in three-dimensional space, the hexagonal close-packed lattice (hcp lattice) has the basal plane with sixfold symmetry and twofold symmetry in the perpendicular plane. The anisotropic functions $d(\theta, \phi)$ and $\tilde{\beta}(\theta, \phi)$ for the crystal with hcp lattice cannot be obtained from equations (2.3) and (2.4).

(b) Nonlinear theory

Simultaneously imposing both anisotropies for capillary force $d(\theta, \theta_d)$ and atomic kinetics $\tilde{\beta}(\theta, \theta_\beta)$, equation (2.5), on the dendrite interface is one of the distinguishing features of the analysis suggested in the works of Saito *et al.* [42] and Brener [43]. On the one hand, most of the analytical works [24,26,27,39] analyse stability conditions in the simple case of surface tension anisotropy mainly for a cubic crystal symmetry. These works predict that dendrites will grow along the direction of the minimum of surface energy, which is verified in experiments with relatively sluggish kinetics in slightly supersaturated or supercooled mixtures and species [88,89]. On the other hand, the focus of the present work lies in the description of the whole measurable range of undercoolings, temperature gradients, cooling rates and solidification velocities on the basis of a unified approach. Therefore, in addition to surface tension anisotropy given by the function $d(\theta, \theta_d)$, anisotropy of the kinetic coefficient $\tilde{\beta}(\theta, \theta_\beta)$ is introduced, which relates interfacial undercooling to local growth velocity, usually valuable at high solidification rates. As a result, the introduction of these two anisotropies, $d(\theta, \theta_d)$ and $\tilde{\beta}(\theta, \theta_\beta)$, allows us to cover the whole spectrum of growth velocities [25,43]: from surface energy controlled growth up to kinetically limited growth of a dendrite.

Simultaneously introducing two anisotropies may, however, lead to a formal difficulty in the mathematical consistency of the present analysis. As a starting point, we have used the linearized equations (3.7) to get the critical wavelength (3.10) as a result of a linear response to the imposed set of perturbations. Simultaneously introducing two anisotropies as small parameters of the theory may lead, however, to an absence of linear responses in the general case and to the unsuitability of the linear stability analysis. Indeed, while the selection problem is investigated in the simple case of surface tension anisotropy [24,26,27,39] with the only small parameter, α_d, the use of linearized equations for perturbations and the Fredholm alternative [90,91] leads to formally correct scaling laws (even though the prefactors for these laws are not determined accurately and they should be obtained from asymptotic solutions or experimental data [25]). Introducing a second small parameter may lead to unreliability of the linearized equations due to structural instability of the theory [92] and a rigorous approach would consist in using matched asymptotics beyond all orders [93]. Hence, the analysis of two small anisotropies of surface tension and kinetics should be rigorously executed in a nonlinear approximation to predict the scaling laws with a dominant role of the surface energy or atomic kinetics.

A rigorous method allowing one to treat the selection theory with nonlinear equations of motion has been developed by Kassner *et al.* for dendrite growth in a forced potential flow [94] and under Oseen flow [95]. Indeed, the Nash–Glicksman integral formulation of the pattern formation problem [93] does not allow the analysis of nonlinear bulk equations that render, for instance, convection intractable. As such, Kassner *et al.* [94–96] extended the nonlinear formulation of the pattern formation problem by its re-formulation in terms of partial differential equations alone. One of the formal advantages of this extended method of Kassner *et al.* is that it paves the way for rigorous nonlinear asymptotic analysis which might be correctly applied to the problem involving multiple parameters [92].

In the present work, a linear analysis of Pelcé *et al.* [27,29] has been extended to high growth velocity with the imposition of two anisotropies (surface tension and kinetics). Such an application of the linear analysis is one attempt to develop a unified approach by stitching together the asymptotics for different effects and phenomena. Obviously, the linear analysis possesses a lower analytical complexity than a rigorous nonlinear analysis [94–96]; however, it allows us to obtain results faster. The lower analytic complexity and faster obtained results are achieved, however, at the price that the stability criteria (3.20) and (5.13) are found without the required formal rigour with respect to a necessarily chosen multi-parametric space. Therefore, derivation of criteria using a nonlinear theory [94–96] on the one hand and numerical tests of the type of [54,55] on the other hand may provide corrections to the stability criteria describing the whole spectrum of dendrite growth velocity.

8. Conclusion

The model for n-fold symmetric dendrites growing under convective flow has been formulated and critically reviewed. Using linear stability analysis and solvability condition, the selection criterion for thermally and solutally controlled growth of the dendrite has been found. A solely kinetically limited mode of dendrite growth in comparison with thermally controlled growth has been analysed in terms of the behaviour of dendrite tip velocity and tip diameter.

A special type of intensive flow leading to convective boundary conditions at the dendrite surface is considered. The obtained selection criterion in the case of convective boundary conditions has been compared with the outcomes following from the conductive boundary conditions at the dendrite surface. The effect of convective heat and mass transport on the growth of pure and binary dendrites with four- and sixfold symmetry has been demonstrated.

Presently unresolved problems of dendritic growth have been pointed out. Several remarks on the presently used theory have been formulated with regard to types of flow, anisotropies, simplifications in the formal description of transport phenomena and the linearity of the stability analysis applied to the problem of dendrite growth with multiple small parameters.

Further studies of dendrite growth could be envisaged to verify the models by the following:

— investigations of the joint influence of a tiny amount of impurity and convective transport on the growth kinetics (which is important for a description of dendritic crystals growing under terrestrial and microgravity conditions [6–8]);
— numerical simulations of solidification, taking account of the anisotropic properties of moving crystal–liquid interfaces and convective boundary conditions (which is important to check the differences in the selection criteria at small and large values of growth Péclet numbers [29,30]);
— computational modelling of intensive (even turbulent) flow in the liquid core of a solidifying sample, which provides convective transport (5.1) and (5.2) at the dendrite surface (this is important to check the 'convective' criterion (5.13));
— checking the transition from the diffusion-limited (solutally and thermally controlled) regime to the kinetically limited regime (which is important to verify theories that predict a smooth/sharp change of the dendrite velocity with the exchange of preferred crystallographic growth direction [12,32,43]);
— direct measurements of the velocity of convective flow *prior to* and during solidification of levitating droplets [69] (this may provide an input of the flow velocity as a measurable parameter into the models with convection as discussed in Galenko *et al*. [36]);
— a comparison of stitching solutions [32] (working in a wide range of undercooling) with exact solutions [94–96] or asymptotic solutions [97] (which provide an analytical description for a narrow range of undercooling); and
— a comparison with experimental and computational data on two-dimensional dendrites with sixfold symmetry (which is important for the description of dendritic patterns appearing in ferroelectric materials under electric fields [98]).

Data accessibility. This article has no additional data.
Authors' contributions. All authors contributed equally to the present review paper.
Competing interests. The authors declare that they have no competing interests.
Funding. This work was supported by the Russian Science Foundation (grant number 16-11-10095) and the German Space Center Space Management (under contract number 50WM1541).

References

1. Chalmers B. 1964 *Principles of solidification*. New York, NY: Wiley.
2. Langer JS. 1980 Instabilities and pattern formation in crystal growth. *Rev. Mod. Phys.* **52**, 1–28. (doi:10.1103/RevModPhys.52.1)

3. Kurz W, Fisher DJ. 1989 *Fundamentals of solidification*. Aedermannsdorf, Switzerland: Trans Tech Publications.
4. Trivedi R, Kurz W. 1994 Dendritic growth. *Int. Mater. Rev.* **39**, 49–74. (doi:10.1179/imr.1994.39.2.49)
5. Galenko PK, Zhuravlev VA. 1994 *Physics of dendrites*. Singapore: World Scientific.
6. Teraoka Y, Saito A, Okawa S. 2002 Ice crystal growth in supercooled solution. *Int. J. Refrig.* **25**, 218–225. (doi:10.1016/S0140-7007(01)00082-2)
7. Yoshizaki I, Ishikawa T, Adachi S, Yokoyama E, Furukawa Y. 2012 Precise measurements of dendrite growth of ice crystals in microgravity. *Microgravity Sci. Technol.* **24**, 245–253. (doi:10.1007/s12217-012-9306-9)
8. Herlach DM, Binder S, Galenko PK, Gegner J, Holland-Moritz D, Klein S, Kolbe M, Volkmann T. 2015 Containerless undercooled melts: ordering, nucleation, and dendrite growth. *Metall. Mater. Trans. A* **46A**, 4921–4936. (doi:10.1007/s11661-015-3052-8)
9. Nersisyan HH, Kim DY, Yoo B, Kang W, Han B, Lee J. 2016 Experimental growth of new 6-fold symmetry patterned microcrystals of AlN: equilibrium structures and growth mechanism. *Cryst. Growth Des.* **16**, 5305–5311. (doi:10.1021/acs.cgd.6b00829)
10. Kahlweit M. 1969 On the dendritic growth of NH_4Br-crystals from aqueous solutions. *J. Cryst. Growth* **5**, 391–394. (doi:10.1016/0022-0248(69)90040-2)
11. Diggle JW, Fredericks RJ, Reimschuessel AC. 1973 Crystallographic and morphological studies of electrolytic zinc dendrites grown from alkaline zincate solutions. *J. Mater. Sci.* **8**, 79–87. (doi:10.1007/BF00755585)
12. Chan SK, Reimer HH, Kahlweit M. 1976 On the stationary growth shapes of NH_4Cl dendrites. *J. Cryst. Growth* **32**, 303–315. (doi:10.1016/0022-0248(76)90111-1)
13. Binder S, Galenko PK, Herlach DM. 2013 Faceting of a rough solid–liquid interface of a metal induced by forced convection. *Phil. Mag. Lett.* **93**, 608–617. (doi:10.1080/09500839.2013.830201)
14. Sun M, Liao H-G, Niu K, Zheng H. 2013 Structural and morphological evolution of lead dendrites during electrochemical migration. *Sci. Rep.* **3**, 3227-1–3227-6. (doi:10.1038/srep03227)
15. Galenko PK, Funke O, Wang J, Herlach DM. 2004 Kinetics of dendritic growth under the influence of convective flow in solidification of undercooled droplets. *Mater. Sci. Eng. A* **375–377**, 488–492. (doi:10.1016/j.msea.2003.10.021)
16. Galenko PK, Binder S, Ehlen GJ. 2012 Forced flow effect on dendritic growth kinetics in a binary nonisothermal system. In *Solidification of containerless undercooled melts* (eds DM Herlach, DM Matson), pp. 349–362. Weinheim, Germany: Wiley-VCH.
17. Alexandrov DV, Galenko PK. 2017 Selected mode of dendritic growth with n-fold symmetry in the presence of a forced flow. *Europhys. Lett.* **119**, 16001. (doi:10.1209/0295-5075/119/16001)
18. Ivantsov GP. 1947 Temperature field around spherical, cylinder and needle-like dendrite growing in supercooled melt. *Dokl. Akad. Nauk SSSR* **58**, 567–569.
19. Ivantsov GP. 1952 On a growth of spherical and needle-like crystals of a binary alloy. *Dokl. Akad. Nauk SSSR* **83**, 573–575.
20. Nash GE, Glicksman ME. 1974 Capillary-limited steady-state dendritic growth—I. Theoretical development. *Acta Metall.* **22**, 1283–1290. (doi:10.1016/0001-6160(74)90141-2)
21. Langer JS, Müller-Krumbhaar H. 1978 Theory of dendritic growth—I. Elements of a stability analysis. *Acta Metall.* **26**, 1681–1687. (doi:10.1016/0001-6160(78)90078-0)
22. Willnecker R, Herlach DM, Feuerbacher B. 1989 Evidence of nonequilibrium processes in rapid solidification of undercooled metals. *Phys. Rev. Lett.* **62**, 2707–2710. (doi:10.1103/PhysRevLett.62.2707)
23. Pelcé P. 1988 *Dynamics of curved fronts*. Boston, MA: Academic Press.
24. Kessler DA, Koplik J, Levine H. 1988 Pattern selection in fingered growth phenomena. *Adv. Phys.* **37**, 255–339. (doi:10.1080/00018738800101379)
25. Brener EA, Mel'nikov VA. 1991 Pattern selection in two-dimensional dendritic growth. *Adv. Phys.* **40**, 53–97. (doi:10.1080/00018739100101472)
26. Langer JS, Hong DC. 1986 Solvability conditions for dendritic growth in the boundary-layer model with capillary anisotropy. *Phys. Rev. A* **34**, 1462–1471. (doi:10.1103/PhysRevA.34.1462)

27. Pelcé P, Bensimon D. 1987 Theory of dendrite dynamics. *Nucl. Phys. B* **2**, 259–270. (doi:10.1016/0920-5632(87)90022-3)
28. Ben Amar M, Pelcé P. 1989 Impurity effect on dendritic growth. *Phys. Rev. A* **39**, 4263–4269. (doi:10.1103/PhysRevA.39.4263)
29. Bouissou Ph, Pelcé P. 1989 Effect of a forced flow on dendritic growth. *Phys. Rev. A* **40**, 6673–6680. (doi:10.1103/PhysRevA.40.6673)
30. Alexandrov DV, Galenko PK. 2013 Selection criterion of stable dendritic growth at arbitrary Péclet numbers with convection. *Phys. Rev. E* **87**, 062403. (doi:10.1103/PhysRevE.87.062403)
31. Alexandrov DV, Galenko PK. 2014 Dendrite growth under forced convection: analysis methods and experimental tests. *Phys.–Usp.* **57**, 771–786. (doi:10.3367/UFNr.0184.201408b.0833)
32. Alexandrov DV, Galenko PK. 2015 Thermo-solutal and kinetic regimes of an anisotropic dendrite growing under forced convective flow. *Phys. Chem. Chem. Phys.* **17**, 19 149–19 161. (doi:10.1039/c5cp03018h)
33. Alexandrov DV, Pinigin DA. 2013 Selection of stable growth conditions for the parabolic dendrite tip in crystallization of multicomponent melts. *Tech. Phys.* **58**, 309–315. (doi:10.1134/S106378421303002X)
34. Alexandrov DV, Galenko PK. 2013 Selection criterion for the growing dendritic tip at the inner core boundary. *J. Phys. A: Math. Theor.* **46**, 195101. (doi:10.1088/1751-8113/46/19/195101)
35. Alexandrov DV, Danilov DA, Galenko PK. 2016 Selection criterion of a stable dendrite growth in rapid solidification. *Int. J. Heat Mass Transf.* **101**, 789–799. (doi:10.1016/j.ijheatmasstransfer.2016.05.085)
36. Galenko PK, Danilov DA, Reuther K, Alexandrov DV, Rettenmayr M, Herlach DM. 2017 Effect of convective flow on stable dendritic growth in rapid solidification of a binary alloy. *J. Cryst. Growth* **457**, 349–355. (doi:10.1016/j.jcrysgro.2016.07.042)
37. Alexandrov DV, Galenko PK. 2017 Selected mode for rapidly growing needle-like dendrite controlled by heat and mass transport. *Acta Mater.* **137**, 64–70. (doi:10.1016/j.actamat.2017.07.022)
38. Alexandrov DV, Galenko PK. 2017 Dendritic growth with the six-fold symmetry: theoretical predictions and experimental verification. *J. Phys. Chem. Solids* **108**, 98–103. (doi:10.1016/j.jpcs.2017.04.016)
39. Barbieri A, Langer JS. 1989 Predictions of dendritic growth rates in the linearized solvability theory. *Phys. Rev. A* **39**, 5314–5325. (doi:10.1103/PhysRevA.39.5314)
40. Ben Amar M. 1988 Theory of needle-crystal. *Physica D: Nonlinear Phenom.* **31**, 409–423. (doi:10.1016/0167-2789(88)90006-1)
41. Brener E, Melnikov VI. 1995 Velocity selection and instability spectrum in 3D dendritic growth. *J. Exp. Theor. Phys.* **80**, 341–345. See http://www.jetp.ac.ru/cgi-bin/dn/e_080_02_0341.pdf.
42. Saito Y, Goldbeck-Wood G, Müller-Krumbhaar H. 1988 Numerical simulation of dendritic growth. *Phys. Rev. A* **38**, 2148–2157. (doi:10.1103/PhysRevA.38.2148)
43. Brener EA. 1990 Effects of surface energy and kinetics on the growth of needle-like dendrites. *J. Cryst. Growth* **99**, 165–170. (doi:10.1016/0022-0248(90)90505-F)
44. Lamb (Sir) H. 1945 *Hydrodynamics*. New York, NY: Dover Publications.
45. Kochin NE, Kibel IA, Roze NV. 1964 *Theoretical hydromechanics*. New York, NY: Interscience.
46. Dash SK, Gill WN. 1984 Foced convection heat and momentum transfer to dendritic structures (parabolic cylinders and paraboloids of revolution). *Int. J. Heat Mass Transf.* **27**, 1345–1356. (doi:10.1016/0017-9310(84)90062-0)
47. Horvay G, Cahn JW. 1961 Dendritic and spheroidal growth. *Acta Metall.* **9**, 695–705. (doi:10.1016/0001-6160(61)90008-6)
48. McFadden GB, Coriell SR, Sekerka RF. 2000 Analytic solution for a non-axisymmetric isothermal dendrite. *J. Cryst. Growth* **208**, 726–745. (doi:10.1016/S0022-0248(99)00478-9)
49. Galenko PK, Alexandrov DV, Titova EA. 2018 The boundary integral theory for slow and rapid curved solid/liquid interfaces propagating into binary systems. *Phil. Trans. R. Soc. A* **376**, 20170218. (doi:10.1098/rsta.2017.0218)
50. Fröman N, Fröman PO. 1965 *JWKB approximation: contributions to the theory*. Amsterdam, The Netherlands: North-Holland.

51. Zel'dovich AB, Istratov AG, Kidin NI, Librovich VB. 1980 Flame propagation in tubes: hydrodynamics and stability. *Combust. Sci. Technol.* **24**, 1–13. (doi:10.1080/00102208008952419)
52. Caroli B, Caroli C, Roulet B, Langer JS. 1986 Solvability condition for needle crystals at large undercooling in a nonlocal model of solidification. *Phys. Rev. A* **33**, 442–452. (doi:10.1103/PhysRevA.33.442)
53. Bouissou P, Perrin B, Tabeling P. 1989 Influence of an external flow on dendritic crystal growth. *Phys. Rev. A* **40**, 509–519. (doi:10.1103/PhysRevA.40.509)
54. Tong X, Beckermann C, Karma A, Li Q. 2001 Phase-field simulations of dendritic crystal growth in a forced flow. *Phys. Rev. E* **63**, 061601. (doi:10.1103/PhysRevE.63.061601)
55. Jeong J-H, Goldenfeld N, Dantzig JA. 2001 Phase field model for three-dimensional dendritic growth with fluid flow. *Phys. Rev. E* **64**, 041602. (doi:10.1103/PhysRevE.64.041602)
56. Gao J, Han M, Kao A, Pericleous K, Alexandrov DV, Galenko PK. 2016 Dendritic growth velocities in an undercooled melt of pure nickel under static magnetic fields: a test of theory with convection. *Acta Mater.* **103**, 184–191. (doi:10.1016/j.actamat.2015.10.014)
57. Brener EA, Mel'nikov VI. 1990 Two-dimensional dendritic growth at arbitrary Peclet number. *J. Phys. France* **51**, 157–166. (doi:10.1051/jphys:01990005102015700)
58. Müller-Krumbhaar H, Abel T, Brener E, Hartmann M, Eissfeldt N, Temkin D. 2002 Growth-morphologies in solidification and hydrodynamics. *JSME Int. J., Ser. B* **45**, 129–132. (doi:10.1299/jsmeb.45.129)
59. Bragard J, Karma A, Lee YH, Plapp M. 2002 Linking phase-field and atomistic simulations to model dendritic solidification in highly undercooled melts. *Interface Sci.* **10**, 121–136. (doi:10.1023/A:1015815928191)
60. Nestler B, Danilov D, Galenko P. 2005 Crystal growth of pure substances: phase-field simulations in comparison with analytical and experimental results. *J. Comput. Phys.* **207**, 221–239. (doi:10.1016/j.jcp.2005.01.018)
61. McPhee MG, Maykut GA, Morison JH. 1987 Dynamics and thermodynamics of the ice/upper ocean system in the marginal ice zone of the Greenland Sea. *J. Geophys. Res.* **92**, 7017–7031. (doi:10.1029/JC092iC07p07017)
62. Notz D, McPhee MG, Worster MG, Maykut GA, Schlünzen KH, Eicken H. 2003 Impact of underwater-ice evolution on Arctic summer sea ice. *J. Geophys. Res.* **108**, 3223. (doi:10.1029/2001JC001173)
63. Alexandrov DV, Nizovtseva IG. 2008 Nonlinear dynamics of the false bottom during seawater freezing. *Dokl. Earth Sci.* **419**, 359–362. (doi:10.1134/S1028334X08020384)
64. Alexandrov DV, Nizovtseva IG. 2008 To the theory of underwater ice evolution, or nonlinear dynamics of 'false bottoms'. *Int. J. Heat Mass Transf.* **51**, 5204–5208. (doi:10.1016/j.ijheatmasstransfer.2007.11.061)
65. Alexandrov DV, Malygin AP. 2011 Convective instability of directional crystallization in a forced flow: the role of brine channels in a mushy layer on nonlinear dynamics of binary systems. *Int. J. Heat Mass Transf.* **54**, 1144–1149. (doi:10.1016/j.ijheatmasstransfer.2010.11.008)
66. Feltham DL, Worster MG, Wettlaufer JS. 2002 The influence of ocean flow on newly forming sea ice. *J. Geophys. Res.* **107**, 3009. (doi:10.1029/2000JC000559)
67. Alexandrov DV, Bashkirtseva IA, Malygin AP, Ryashko LB. 2013 Sea ice dynamics induced by external stochastic fluctuations. *Pure Appl. Geophys.* **170**, 2273–2282. (doi:10.1007/s00024-013-0664-z)
68. Hyers RW, Trapaga G, Abedian B. 2003 Laminar–turbulent transition in an electromagnetically levitated droplet. *Metall. Mater. Trans. B* **34B**, 29–36. (doi:10.1007/s11663-003-0052-7)
69. Lee J, Matson DM, Binder S, Kolbe M, Herlach D, Hyers RW. 2014 Magnetohydrodynamic modeling and experimental validation of convection inside electromagnetically levitated Co–Cu droplets. *Metall. Mater. Trans. B* **45B**, 1018–1023. (doi:10.1007/s11663-013-9995-5)
70. Gao J, Kao A, Bojarevics V, Pericleous K, Galenko PK, Alexandrov DV. 2017 Modeling of convection, temperature distribution and dendritic growth in glass-fluxed nickel melts. *J. Cryst. Growth* **471**, 66–72. (doi:10.1016/j.jcrysgro.2016.11.069)
71. Tritton DJ 1988 *Physical fluid dynamics*. Oxford, UK: Clarendon Press.

72. Owen PR, Thomson WR. 1963 Heat transfer across rough surfaces. *J. Fluid Mech.* **15**, 321–334. (doi:10.1017/S0022112063000288)
73. Yaglom AM, Kader BA. 1974 Heat and mass transfer between a rough wall and turbulent flow at high Reynolds and Peclet numbers. *J. Fluid Mech.* **62**, 601–623. (doi:10.1017/S0022112074000838)
74. Alexandrov DV, Nizovtseva IG, Lee D, Huang H-N. 2010 Solidification from a cooled boundary with a mushy layer under conditions of nonturbulent and turbulent heat and mass transfer in the ocean. *Int. J. Fluid Mech. Res.* **37**, 1–14. (doi:10.1615/InterJFluidMechRes.v37.i1.10)
75. Bojarevics V, Kao A, Pericleous K. 2012 Modeling of fluid dynamics and dendritic solidification in EM-levitated alloy melts. In *Solidification of containerless undercooled melts* (eds DM Herlach, DM Matson), pp. 321–348. Weinheim, Germany: Wiley-VCH.
76. Binder S, Galenko PK, Herlach DM. 2014 The effect of fluid flow on the solidification of Ni_2B from the undercooled melt. *J. Appl. Phys.* **115**, 053511. (doi:10.1063/1.4864151)
77. Beckermann C, Diepers HJ, Steinbach I, Karma A, Tong X. 1999 Modeling melt convection in phase-field simulations of solidification. *J. Comput. Phys.* **154**, 468–496. (doi:10.1006/jcph.1999.6323)
78. Mullis AM, Dragnevski K, Cochrane RF. 2004 Mechanically deformed primary dendritic structures observed during the solidification of undercooled melts. In *Solidification and crystallization* (ed. DM Herlach), pp. 175–184. Weinheim, Germany: Wiley-VCH.
79. Galenko PK, Reuther K, Kazak OV, Alexandrov DV, Rettenmayr M. 2017 Effect of convective transport on dendritic crystal growth from pure and alloy melts. *Appl. Phys. Lett.* **111**, 031602. (doi:10.1063/1.4985340)
80. Koss MB, LaCombe JC, Tennenhouse LA, Glicksman ME, Winsa EA. 1999 Dendritic growth tip velocities and radii of curvature in microgravity. *Metall. Mater. Trans. A* **30**, 3177–3190. (doi:10.1007/s11661-999-0228-0)
81. Hartmann H, Galenko PK, Holland-Moritz D, Kolbe M, Herlach DM, Shuleshova O. 2008 Nonequilibrium solidification in undercooled $Ti_{45}Al_{55}$ melts. *J. Appl. Phys.* **103**, 073509. (doi:10.1063/1.2903920)
82. Galenko PK, Herlach DM, Funke O, Phanikumar G. 2004 Phase-field modelling of dendritic solidification: verification of the model predictions with latest experimental data. In *Solidification and crystallization* (ed. DM Herlach), pp. 52–60. Weinheim, Germany: Wiley-VCH.
83. Galenko PK, Herlach DM. 2008 Dendrite growth and grain refiniment in undercooled melts. In *Phase transformations in multicomponent melts* (ed. DM Herlach), pp. 353–772. Weinheim, Germany: Wiley-VCH.
84. Biloni H, Boettinger WJ. 1996 Solidification. In *Physical metallurgy* (eds RW Cahn, P Haasen), 4th edn, vol. 1, pp. 669–842. Amsterdam, The Netherlands: Elsevier.
85. Eckler K, Herlach DM. 1994 Measurements of dendrite growth velocities in undercooled pure Ni-melts—some new results. *Mater. Sci. Eng. A* **178**, 159–162. (doi:10.1016/0921-5093(94)90535-5)
86. Funke O, Phanikumar G, Galenko PK, Chernova L, Reutzel S, Kolbe M, Herlach DM. 2006 Dendrite growth velocity in levitated undercooled nickel melts. *J. Cryst. Growth* **297**, 211–222. (doi:10.1016/j.jcrysgro.2006.08.045)
87. Galenko PK, Danilov DA. 1997 Local nonequilibrium effect on rapid dendritic growth in a binary alloy melt. *Phys. Lett. A* **235**, 271–280. (doi:10.1016/S0375-9601(97)00562-8)
88. Ben-Jackob E, Godbey R, Goldenfeld ND, Koplik J, Levin H, Mueller TE, Sander LM. 1985 Experimental demonstration of the role of anisotropy in interfacial pattern formation. *Phys. Rev. Lett.* **55**, 1315–1318.(doi:10.1103/PhysRevLett.55.1315)
89. Dougherty A, Gollub J. 1988 Steady-state dendritic growth of NH_4Br from solution. *Phys. Rev. A* **38**, 3043–3053. (doi:10.1103/PhysRevA.38.3043)
90. Kantorovich L, Akilov G. 1964 *Functional analysis in normed spaces*. New York, NY: Macmillan.
91. Rudin W. 1973 *Functional analysis*. New York, NY: McGraw-Hill.
92. Tanveer S. 1989 Analytic theory for the selection of a two-dimensional needle crystal at arbitrary Péclet number. *Phys. Rev. A* **40**, 4756–4769. (doi:10.1103/PhysRevA.40.4756)
93. Kruskal MD, Segur H. 1991 Asymptotics beyond all orders in a model of crystal growth. *Stud. Appl. Math.* **85**, 129–181. (doi:10.1002/sapm1991852129)

94. Fischaleck T, Kassner K. 2008 Extending the scope of microscopic solvability: combination of the Kruskal–Segur method with Zauderer decomposition. *Europhys. Lett.* **81**, 54004. (doi:10.1209/0295-5075/81/54004)
95. Von Kurnatowski M, Kassner K. 2014 Scaling laws of free dendritic growth in a forced Oseen flow. *Phys. Rev. E* **47**, 325202. (doi:10.1088/1751-8113/47/32/325202)
96. Von Kurnatowski M, Grillenbeck T, Kassner K. 2013 Selection theory of free dendritic growth in a potential flow. *Phys. Rev. E* **87**, 042405. (doi:10.1103/PhysRevE.87.042405)
97. Brener E. 1999 Pattern formation in three-dimensional dendritic growth. *Physica A* **263**, 338–344. (doi:10.1016/S0378-4371(98)00488-9)
98. Shur VY, Akhmatkhanov AR, Pelegova EV. 2016 Self-organizing formation of dendrite domain structures in lithium niobate and lithium tantalate crystals. *Ferroelectrics* **500**, 76–89. (doi:10.1080/00150193.2016.122911)